Mon. Not. R. Astron. Soc. **327,** 141–168 (2001)

Chemical abundances of planetary nebulae from optical recombination lines – III. The Galactic bulge PN M 1-42 and M 2-36

X.-W. Liu,[1,2]★ S.-G. Luo,[2] M. J. Barlow,[1] I. J. Danziger[3] and P. J. Storey[1]

[1]*Department of Physics and Astronomy, University College London, Gower Street, London WC1E 6BT*
[2]*Department of Astronomy, Peking University, Beijing 100871, China*
[3]*Osservatorio Astronomico di Trieste, Via G. B. Tiepolo 11, I-34131 Trieste, Italy*

Accepted 2001 May 23. Received 2001 April 2

ABSTRACT

We present deep, high-resolution optical spectra of two Galactic bulge planetary nebulae (PN), M 1-42 and M 2-36. The spectra show very prominent and rich optical recombination lines (ORLs) from C, N, O and Ne ions. Infrared spectra from 2.4–197 μm were also obtained using the Short and Long Wavelength Spectrometer (SWS and LWS) on board *ISO*. The optical and infrared spectra, together with archival *IUE* spectra, are used to study their density and thermal characteristics and to determine elemental abundances.

We determine the optical and UV extinction curve towards these two bulge PN using observed H I and He II recombination line fluxes and the radio free–free continuum flux density. In the optical, the reddening curve is found to be consistent with the standard Galactic extinction law, with a total to selective extinction ratio $R \equiv A(V)/E(B-V) = 3.1$. However, the extinction in the UV is found to be much steeper, consistent with the earlier finding of Walton, Barlow & Clegg.

The rich ORL spectra from C, N, O and Ne ions detected from the two nebulae have been used to determine the abundances of these elements relative to hydrogen. In all cases, the resultant ORL abundances are found to be significantly higher than the corresponding values deduced from collisionally excited lines (CELs). In M 2-36, the discrepancies are about a factor of 5 for all four elements studied. In M 1-42, the discrepancies reach a factor of about 20, the largest ever observed in a PN. M 1-42 also has the lowest Balmer jump temperature ever determined for a PN, $T_e(\mathrm{BJ}) = 3560$ K, 5660 K lower than its [O III] forbidden line temperature.

We compare the observed intensities of the strongest O II ORLs from different electronic configurations, including λ4649 from 3s–3p, λ4072 from 3p–3d, λ4089 from 3d–4f, and λ4590 and λ4190 from the doubly excited 3s′–3p′ and 3p′–3d′ configurations, respectively. In all cases, in spite of the fact that the ratios of the ORL to CEL ionic abundances span a wide range from ∼5–20, the intensity ratios of λ4649, λ4072, λ4590 and λ4190 relative to λ4089 are found to be nearly constant, apart from some small monotonic increase of these ratios as a function of electron temperature. Over a range of Balmer jump temperature from 3500–8100 K, the variations amount to about 20 per cent for the 3s–3p and 3p–3d transitions and a factor of 2 for the primed transitions, and are consistent with the predictions of the current recombination theory. Our results do not support the claim by Dinerstein, Lafon & Garnett that the relative intensities of O II ORLs vary from nebula to nebula and that the scatter is largest in objects where the discrepancies between ORL and CEL abundances are also the largest.

We find that the ORL to CEL abundance ratio is highly correlated with the difference between the temperatures yielded by the [O III] forbidden line ratio and by the H I Balmer jump, providing the strongest evidence so far that the two phenomena, i.e. the disparity between ORL and CEL temperature and abundance determinations, are closely related.

★E-mail: xwl@star.ucl.ac.uk

However, temperature fluctuations of the type envisaged by Peimbert are unable to explain the low ionic abundances yielded by IR fine-structure lines. The very low Balmer jump temperature of M 1-42, coupled with its very low Balmer decrement density, may also be difficult to explain with a chemically inhomogeneous composite model of the type proposed by Liu et al. for NGC 6153.

Key words: ISM: abundances – planetary nebulae: individual: M 1-42 – planetary nebulae: individual: M 2-36.

1 INTRODUCTION

In Paper I (Liu et al. 2000), we presented C, N, O and Ne elemental abundances derived from optical recombination lines (ORLs) for the planetary nebula (PN) NGC 6153, and found that the ORL abundances were all approximately a factor of 10 higher than those derived using the traditional method based on collisionally excited lines (CELs). These discrepancies between the heavy element abundances derived from these two types of emission line in NGC 6153 were a factor of 2 larger than those reported previously by us for the Saturn nebula NGC 7009 (Liu et al. 1995). We found that temperature and/or density fluctuations alone failed to explain all the observational patterns, unless the nebula is also chemically inhomogeneous. We showed that H-deficient inclusions, with properties possibly similar to those found in 'born-again' PN such as A 30, embedded in a nebula of more or less 'normal' elemental abundances, may provide a viable solution to the very large discrepancies observed for this nebula. In the second paper of this series (Luo, Liu & Barlow 2001), we presented determinations of the Ne abundance for the Saturn nebula using both ORLs and optical and infrared CELs and found that the Ne/H abundance ratio derived from Ne II ORLs is again much higher than those derived from CELs, by approximately the same factor as found previously by us for C, N and O.

In this paper we present deep optical spectroscopy for two Galactic bulge PN, M 1-42 and M 2-36. Ionic abundances of C, N, O and Ne are derived from ORLs and compared to those derived from UV, optical and IR CELs. M 1-42 and M 2-36 are singled out because, during our deep optical spectroscopic survey of a large sample of Galactic PN, both nebulae were found to have a very prominent ORL spectrum from CNO and Ne ions, remarkably similar to those observed from NGC 7009 and 6153. As we will show in this paper, the ORL ionic abundances derived for M 1-42 and M 2-36 are respectively, about a factor of 20 and 5 higher than those derived from CELs. The discrepancy of a factor 20 in M 1-42 is the largest that has ever been observed in a PN. PN with discrepancies larger than a factor of 5 between the ionic abundances derived from ORLs and CEls are relatively rare. Of the approximately 80 Galactic PN surveyed by us, only a few such nebulae have been identified. Detailed abundance studies of this small group of nebulae are nevertheless extremely important, as the analyses may provide an insight into the underlying physics that can lead to the abundance determination discrepancy between the two types of emission lines. This discrepancy has been observed in many PN, although in most cases, the magnitude of the discrepancy is much smaller, typically a factor of 2–3 (Liu et al. 1999). The large number of ORLs detected from each ionic species in the optical spectra of the extreme nebulae also provides a unique opportunity to test the recombination theory of non-hydrogenic ions.

M 1-42 (PN G002.7−04.8) and M 2-36 (PN G003.2−06.2) were discovered by Minkowski on objective-prism survey plates obtained by W. C. Miller with the Mount Wilson Observatory 10-inch telescope (Minkowski 1946, 1947). M 1-42 and M 2-36 have angular diameters of 9 and 8 arcsec, respectively (Kinman, Feast & Lasker 1988; Moreno et al. 1988; Zijlstra, Pottasch & Bignell 1989) and 1.4 GHz radio free–free continuum fluxes of 29 and 23 mJy (Condon & Kaplan 1998). Both nebulae are located within 10° of the Galactic centre and have very large radial velocities ($V_{\rm lsr} = -84$ and 111 km s^{-1} for M 1-42 and M 2-36, respectively; Schneider et al. 1983). As a result, both are classified as Galactic bulge PN in the Strasbourg-ESO Catalogue of Galactic Planetary Nebulae (Acker et al. 1992).

Section 2 describes the observations and presents the measured line fluxes. Apart from optical spectroscopy, we have also observed both nebulae using the Short and Long Wavelength Spectrometers (SWS and LWS) on board the *Infrared Space Observatory* (*ISO*). The IR spectra cover 2.4–197 μm and yield fluxes for many collisionally excited fine-structure lines. Archival *International Ultraviolet Explorer* (*IUE*) spectra are available for both nebulae and are included in the current analysis. Dust extinction towards the Galactic bulge has been reported to differ significantly from the standard reddening curve for the diffuse interstellar medium, particularly in the UV wavelength region (Walton et al. 1993). We have thus carried out a detailed extinction analysis towards M 1-42 and M 2-36 using fresh data presented in this paper and derive the extinction curve towards the two nebulae (Section 3). Plasma diagnostic analyses are presented in Section 4. In Section 5, we present the ionic abundances derived from both ORLs and CELs and discuss the results in Section 6.

2 OBSERVATIONS

2.1 Optical spectroscopy

M 1-42 and M 2-36 were observed at the European Southern Observatory (ESO) 1.52-m telescope using the B&C spectrograph in 1995 July and 1996. A journal of the observations is given in Table 1. In 1995 the detector was a Ford 2048 × 2048 15 μm × 15 μm charge coupled device (CCD), which was superseded in 1996 by a thinned UV-enhanced Loral 2048 × 2048 15 μm × 15 μm chip of much improved quantum efficiency (about a factor of 5 at 4000 Å). The B&C spectrograph has a useful slit length of about 3.5 arcmin. During both runs, the CCDs were binned by a factor of 2 along the slit direction in order to reduce the CCD readout noise. A slit width of 2 arcsec was used for nebular observations. A low-resolution spectrum of short exposure time was also obtained for each object with an 8-arcsec wide slit.

The spectra were reduced with standard procedures using the LONG92 package in MIDAS.[1] The spectra were bias-subtracted, flat-fielded and cosmic-rays removed, and then wavelength calibrated

[1] MIDAS is developed and distributed by the European Southern Observatory.

using exposures of a He–Ar calibration lamp. The spectra were flux calibrated using wide-slit (8 arcsec) observations of the *Hubble Space Telescope* (*HST*) standard stars Feige 110 and the nucleus of PN NGC 7293. Ozone absorption bands which affect data shortwards of 3400 Å were corrected for using 2-arcsec wide-slit observations of the two standard stars. Further details about the instrumental setups and data reduction can be found in Liu et al. (2000).

Fig. 1 shows the spectra of M 1-42 and M 2-36, from the atmospheric cut-off to Hβ, after integration along the slit. Note the strength of the interstellar Ca II K absorption line at 3933.66 Å. In M 2-36, the peak absorption of the Ca II H line falls nearly exactly (within $\lesssim 0.1$ Å) at the wavelength of the [Ne III] λ3967 nebular emission line, suppressing the intensity of the latter by nearly a factor of 2, whereas in M 1-42, about one third of the Hϵ nebular emission has been removed by the interstellar Ca II H line.

The observed line fluxes, normalized such that $F(\mathrm{H}\beta) = 100$, are presented in Table 2. M 1-42 has an observed continuum flux (again in units where $\mathrm{H}\beta = 100$) at 3643 and 3681 Å of $F_\mathrm{c}(\lambda3643) = 0.544\,\text{Å}^{-1}$ and $F_\mathrm{c}(\lambda3681) = 0.086\,\text{Å}^{-1}$, respectively, or $I_\mathrm{c}(\lambda3643) = 1.012\,\text{Å}^{-1}$ and $I_\mathrm{c}(\lambda3681) = 0.156\,\text{Å}^{-1}$ after correction for reddening (cf. Section 3). Thus we have $\mathrm{BJ/H\,11} \equiv [I_\mathrm{c}(\lambda3643) - I_\mathrm{c}(\lambda3681)]/I(\mathrm{H\,11}\lambda3770) = 0.230$ Å and $\mathrm{BJ/H}\beta \equiv [I_\mathrm{c}(\lambda3643) - I_\mathrm{c}(\lambda3681)]/I(\mathrm{H}\beta) = 8.56 \times 10^{-3}$ Å. Similarly, for M 2-36, $F_\mathrm{c}(\lambda3643) = 0.530\,\text{Å}^{-1}$, $F_\mathrm{c}(\lambda3681) = 0.105\,\text{Å}^{-1}$, $I_\mathrm{c}(\lambda3643) = 0.765\,\text{Å}^{-1}$, $I_\mathrm{c}(\lambda3681) = 0.149\,\text{Å}^{-1}$, so we have $\mathrm{BJ/H\,11} = 0.162$ Å and $\mathrm{BJ/H}\beta = 6.16 \times 10^{-3}$ Å. A weak discontinuity at 3421 Å, produced by recombination of singly ionized helium to the He I $2\,^3$P state, has been detected in both nebulae (Fig. 1). The discontinuity is most clearly seen in the spectrum of M 2-36, which has a better signal-to-noise (S/N) ratio. Accurate measurement of this discontinuity is however difficult.

2.2 Infrared spectroscopy

M 1-42 and M 2-36 were observed with the SWS and LWS on board the *ISO* on 1997 October 19, during *ISO* orbit #703. The SWS observations were carried out using the SWS01 observing template AOT1 in speed 2 for full wavelength grating scans. The *ISO* data product numbers (TDT) for the SWS spectra of M 1-42 and M 2-36 are 70302306 and 70302403, respectively. The spectra cover 2.4–45 μm at a degraded spectral resolution of approximately 200. The total on-target exposure time was 2124 s for each nebula. The spectra, processed with the SWS Off-line Pipeline (OLP) Version 8.7, were retrieved from the *ISO* data archive at the European Space Agency (ESA) centre at Vilspa. The angular sizes of M 1-42 and M 2-36 are small enough to fit into the SWS entrance aperture, which has a size of 14×20 arcsec^2 for bands 1–2 (2.4–12 μm) and is even larger for the longer wavelength bands 3–4.

The observed fluxes of the fine-structure lines detected in the SWS spectra of M 1-42 and M 2-36 are presented in Table 3. The [Ne III] 36-μm line in M 1-42 was only marginally detected and its flux is subject to large uncertainties of a factor 2 or more. The [S III] 18.7-μm and 33.5-μm line fluxes of M 1-42 are also uncertain, with estimated errors of about 30–50 per cent. For other well detected lines, the flux uncertainties are probably dominated by systematic errors, which are probably less than 20 per cent. For M 2-36, the formal flux uncertainties as estimated from Gaussian line profile fitting are about 30 per cent for the [Ar III] 9.0-μm, [S III] 33.5-μm and [Ne III] 36.0-μm lines and are less than 15 per cent for other stronger lines. The [Ne III] 15.6-μm line in the downward-scan spectrum of M 2-36 was seriously affected by cosmic ray hits and all data points were rejected by the OLP during the auto-processing. A few data points in the blue wing of the [Ne III] 15.6-μm line were also affected in the upward-scan spectrum. The flux of this line given in Table 3 for M 2-36 was derived from Gaussian profile fitting to the upward-scan spectrum only.

The LWS observations were carried out with the LWS AOT01, which yields full wavelength grating scans from 43–197 μm at a spectral resolution of $\sim$200. The TDTs for the M 1-42 on- and off-source spectra are 70302104 and 70302105, respectively. For the M 2-36 on- and off-source spectra, the TDTs are 70302001 and 70302002, respectively. For the on-source spectra of both nebulae, the total on-target exposure time was 2441 s, which yielded 12 scans. For the off-source spectra, only six scans were obtained, with a total on-target exposure time of 1381 s. The off-source spectrum of M 1-42 was taken 10 arcmin north of the nebula. For M 2-36, the off-source spectrum was obtained 7 arcmin south of the nebula. The on- and off-source LWS spectra of M 1-42 were flagged as 'Failed' in the *ISO* archive because of the presence of some broad emission features at wavelengths longer than 140 μm, affecting in particular the [C II] 158-μm line. The origin of these artificial features is still unknown. However, nebular emission lines at shorter wavelengths are probably not affected. The LWS data were processed with the LWS Version 7 OLP. For a given wavelength, data from individual scans were averaged and deviant points clipped. There are significant overlaps in the wavelength coverage between the subspectra recorded on the 10 LWS detectors, allowing all detected lines, except for the [N II] 122-μm line, to be measured twice, on two adjacent detectors. For each line, the two measurements from adjacent detectors generally agreed very well and were therefore averaged according to the S/N. There is no discernible emission of the [O III] 52- and 88-μm and the [N III] 57-μm lines in the background spectra of M 1-42 and M 2-36. For these three lines, we have adopted measurements made directly on the on-source spectra, without subtracting the corresponding off-source spectra. Excluding possible systematic errors in flux calibration, the uncertainties in the fluxes of the three lines are estimated at $\sim$5 and 10 per cent for M 1-42 and M 2-36, respectively. For the [N II] 122-μm and [O I] 63-μm lines, there are some small contributions from the Galactic background emission. Their fluxes were therefore measured after subtracting the off-source spectra from the on-source ones. The 63-μm line fluxes are probably accurate to 15 per cent, whereas the 122-μm line flux of M 1-42 is probably accurate to 25 per cent. For both nebulae, the [C II] 158-μm emission detected in the on-source spectra is entirely because of the Galactic background emission. M 1-42 and M 2-36 were included in a sample of 52 PN observed with the LWS for which the fine-structure line fluxes have been published by Liu et al. (2001). Some of the fluxes presented in Table 3 differ slightly from those published by Liu et al. (2001). The differences are always insignificant compared to the actual measurement errors and were caused by the slightly different analysis procedure.

The *ISO* SWS and LWS fluxes of M 1-42 were normalized to $\mathrm{H}\beta = 100$ using a dereddened Hβ flux of $\log I(\mathrm{H}\beta) = \log F(\mathrm{H}\beta) + c = -11.63 + 0.70 = -10.93$ (erg cm^{-2} s^{-1}). Similarly, for M 2-36, the infrared line fluxes were normalized using $\log I(\mathrm{H}\beta) = -11.18$ (erg cm^{-2} s^{-1}). The extinction corrections are discussed in Section 3.

2.3 *IUE* observations

M 1-42 and M 2-36 were observed by us with the *IUE* on 1990 August 14 and 1993 August 6, respectively, using the Short

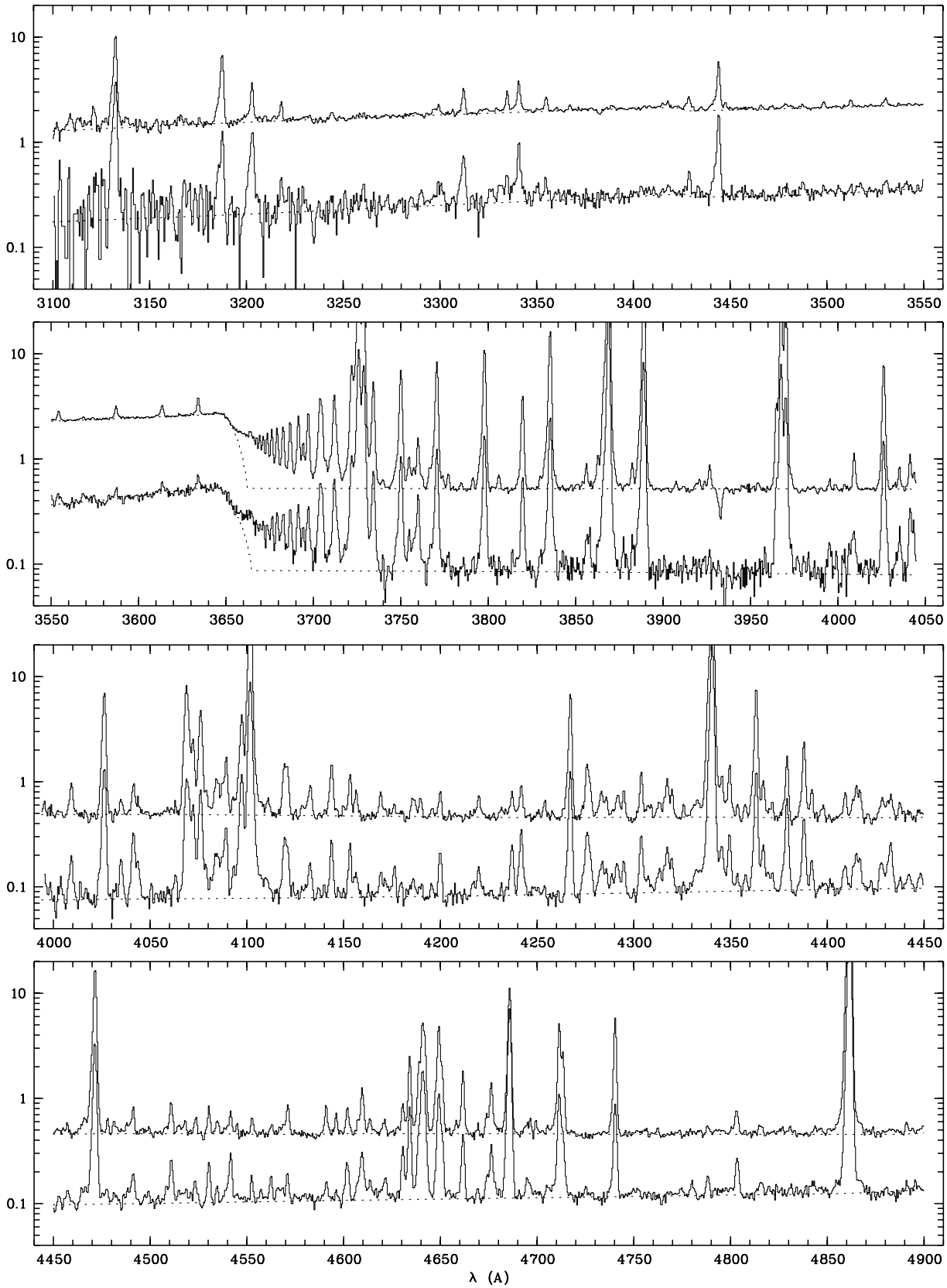

Figure 1. Optical spectra of M 1-42 (lower curve) and M 2-36 (upper curve, scaled up by a factor of 5) from the blue atmospheric cut-off to Hβ. The spectra are rich in recombination lines from C, N, O and Ne ions. The dotted lines show the adopted continuum levels. The spectra were corrected to laboratory wavelengths using H I Balmer lines and normalized such that $F(\mathrm{H}\beta) = 100$. Interstellar extinction has not been corrected for. Note the weak He I discontinuity at 3421 Å and the strong interstellar Ca II K absorption line at 3934 Å.

Table 1. Journal of ESO 1.52-m observations[a].

Date (UT)	λ range (Å)	FWHM (Å)	PA (deg)	Exp. time (s)
M 1-42				
30/07/95	3520–7420	4.5	120	60, 300, 60[b]
08/07/96	3994–4983	1.5	120	2 × 1200, 2 × 1800
12/07/96	3040–4048	1.5	120	300, 2 × 1800
M 2-36				
30/07/95	3520–7420	4.5	0	30, 300, 30[b]
31/07/95	4000–4987	1.5	0	2 × 1800
10/07/96	3994–4983	1.5	0	1800
11/07/96	3040–4048	1.5	0	2 × 1800

[a] All observations were taken with a 2-arcsec wide slit except otherwise specified.
[b] Taken with an 8-arcsec wide slit.

Wavelength Prime camera (SWP) with the *IUE* large aperture, an 10.3 × 23 oval. The integration time was 17 099 s for M 1-42 (SWP 39461) and 9899 s (SWP 48319) for M 2-36. The spectra were retrieved from the *IUE* final archive at the ESA centre at Vilspa (Fig. 2). Note the P-Cygni profile of the He II λ1640 line in M 2-36, implying that the line is dominated by emission from the stellar wind of the central star, rather than from the nebula. Measured fluxes of detected lines are given in Table 4. The fluxes are normalized to Hβ = 100 using an observed Hβ flux of $\log F(\mathrm{H}\beta) = -11.63$ and -11.45 (erg cm^{-2} s^{-1}) for M 1-42 and M 2-36, respectively, and then corrected for extinction using the reddening curves given by equations (1) and (2) for M 1-42 and M 2-36, respectively (cf. Section 3). Owing to the lack of an *IUE* flux for the *nebular* He II λ1640 emission line in M 2-36, the UV extinction curve towards this nebula is uncertain. Consequently, the dereddened *IUE* line intensities of M 2-36 given in Table 4 should be treated with some caution.

3 EXTINCTION TOWARDS M 1-42 AND M 2-36

Walton et al. (1993) measured He II λ1640/λ4686 ratios from *IUE* and optical spectra for a sample of Galactic bulge PN. They found that the FUV extinction law towards the Galactic centre is much steeper than for the general interstellar medium (ISM). In the optical, the ratio of total to selective extinction, $R \equiv A(\mathrm{V})/E(B-V)$, was also found to be much smaller – they found that on average $R = 2.3$, compared to the standard value of 3.1 for the general ISM. The lowest value of R found elsewhere in the Galaxy is towards the B3 V star HD 210121, obscured by the high-latitude cloud DBB 80, for which $R = 2.1 \pm 0.2$ has been observed (Welty & Fowler 1992; Larson, Whittet & Hough 1996). The UV and optical reddening law towards the Galactic bulge has not been determined by any other method, because of the lack of suitable luminous early-type stars, such as one traditionally used.

The extinction curve towards M 1-42 and M 2-36 can be derived by comparing the observed Balmer decrement, the He II λ1640/λ4686, and λ3203/λ4686 ratios, and the total Hβ to radio f–f continuum ratio, with the predictions of recombination theory (Storey & Hummer 1995). Since the ratio of the radio continuum flux to Hβ depends weakly on He ionic abundances and electron temperature, a preliminary plasma diagnostic and abundance analysis was carried out assuming the standard ISM reddening law (Howarth 1983). This yielded $T_e(\mathrm{BJ}) = 4000$ K, $\mathrm{He}^+/\mathrm{H}^+ = 0.149$ and $\mathrm{He}^{2+}/\mathrm{H}^+ = 0.011$ for M 1-42. For M 2-36 we obtained $T_e(\mathrm{BJ}) = 5000$ K, $\mathrm{He}^+/\mathrm{H}^+ = 0.134$ and $\mathrm{He}^{2+}/\mathrm{H}^+ = 0.003$. These values were then used to calculate the intrinsic ratio of the radio continuum flux to Hβ, the Balmer decrement and the He II λ1640/λ4686 and λ3203/λ4686 ratios.

Condon & Kaplan (1998) recently published radio 1.4-GHz fluxes for over 800 Galactic PN, derived from a Very Large Array (VLA) survey of sky north of J2000 declination $\delta = -40°$. They give $S(1.4\,\mathrm{GHz}) = 28.6 \pm 1.0$ and 23.0 ± 0.8 mJy for M 1-42 and M 2-36, respectively. Assuming that both nebulae are optically thin at 1.4 GHz, the observed 1.4 GHz fluxes yield 5-GHz fluxes of $S(5\,\mathrm{GHz}) = 24.2 \pm 0.8$ and 19.5 ± 0.7 mJy, for M 1-42 and M 2-36, respectively, comparable to the values of 24 and 13 mJy measured directly at 5 GHz by Zijlstra et al. (1989). For the total Hβ flux of M 1-42, we have taken the value of $\log F(\mathrm{H}\beta) = -11.63$ (erg cm^{-2} s^{-1}) from the compilation of Cahn, Kaler & Stanghellini (1992). No reliable measurement of $F(\mathrm{H}\beta)$ has been published for M 2-36 and we have adopted the value of $\log F(\mathrm{H}\beta) = -11.45$ (erg cm^{-2} s^{-1}), obtained from our own observation taken with an 8-arcsec slit width. M 2-36 has an optical diameter of 8.″1 (Kinman et al. 1988; Moreno et al. 1988). Thus our wide-slit observation should have included all the Hβ emission from M 2-36, although some small loss of light cannot be ruled out.

The extinction $A(\lambda)$ derived from the above parameters using the observed line fluxes listed in Table 2 are given in Table 5. The Hδ line at 3970 Å from M 1-42 is affected by interstellar Ca H line absorption (cf. Section 2) and was therefore excluded. The He II λ1640 line in M 2-36 is dominated by the stellar wind from the central star and thus cannot be used for reddening determinations. By interpolating values of $A(\lambda)$ at Hα, Hβ and Hγ, we find $A(V) = 1.50$ and $A(B) = 1.96$ for M 1-42, which yield a total-to-selective extinction ratio of $R = 3.3$. Similarly, for M 2-36 we find $A(V) = 0.55$, $A(B) = 0.80$ and $R = 2.3$. Given the lower extinction towards M 2-36, the value of R deduced from it is less reliable than that deduced from M 1-42 – a 30 per cent increase in the adopted Hβ flux of M 2-36 would yield a value of R comparable to the standard ISM value of 3.1. For the adopted electron temperature for M 1-42, Case B recombination predicts a λ1640/λ4686 ratio of 5.65, compared with the observed value of 5.94. By interpolating $A(\lambda)$ at the wavelengths of Hβ and Hγ, we find $A(\lambda 4686) = 1.84$ mag towards M 1-42, which when combined with the observed and predicted ratios of the λ1640/λ4686 ratio yields $A(\lambda 1640) = 5.70$ mag. The extinction at the wavelength of the He II λ3203 was also derived from the observed λ3203/λ4686 ratio. Given the weakness of the λ3203 line and the possible effects of ozone absorption, the extinction derived from this transition will be ignored in our analysis.

The total to selective extinction ratio $R = 3.3$ deduced for M 1-42 is consistent with the standard ISM value. However, the FUV extinction is much steeper than the standard reddening law, consistent with the previous finding of Walton et al. (1993). In Fig. 3 we plot the normalized extinction, $X(x) \equiv E(\lambda - V)/E(B-V)$, as a function of $x \equiv 1/\lambda(\mu\mathrm{m})$. Also shown are the standard Galatic ISM reddening law for $R = 3.1$ (Howarth 1983) and the R-dependent Galatic reddening curves of Cardelli, Clayton & Mathis (1989) for $R = 3.1$ and 2.3. The steep rise of the FUV extinction curve along the line of sight towards M 1-42 is striking.

The extinction $A(\lambda)$ towards M 1-42 can be well fitted by a linear function of $x \equiv 1/\lambda(\mu\mathrm{m})$,

$$A(\lambda) = -0.267 + 0.981x.$$

Table 2. Observed optical line fluxes on a scale where Hβ = 100.

λ_{obs}	M1-42 $F(\lambda)$	$I(\lambda)$	λ_{obs}	M2-36 $F(\lambda)$	$I(\lambda)$	Ion	λ_0	Mult	Lower term	Upper term	g_1	g_2
			3045.72	0.610	1.174	O III	3047.12	V4	3s 3P*	3p 3P	5	5
			3108.93	0.165	0.306	[Ar III]	3109.17	F2	2p4 3P	2p4 1S	3	1
			3117.22	0.111	0.205	Ne II	3117.98	V16	3p 4D*	3d 4P	8	6
			3121.01	0.213	0.393	O III	3121.71	V12	3p 3S	3d 3P*	3	3
3132.21	8.11	22.61	3132.26	3.65	6.70	O III	3132.79	V12	3p 3S	3d 3P*	3	5
3184.95	0.442	1.175	3184.74	0.288	0.514	Si III	3185.12	V8	4p 1P*	5s 1S	3	1
3187.57	2.216	5.877	3187.36	1.964	3.499	He I	3187.74	V3	2s 3S	4p 3P*	3	9
3202.93	2.660	6.959	3202.88	0.687	1.214	He II	3203.10	3.5	3d+ 2D	5f+ 2F*	18	50
			3209.58	0.077	0.136	Ne II	3208.96	V13	3p 4D*	3d 4F	8	8
						Ne II	3209.36	V16	3p 4D*	3d 4P	2	4
			3214.38	0.075	0.132	Ne II	3214.33	V13	3p 4D*	3d 4F	4	6
						Ne II	3213.73	V13	3p 4D*	3d 4F	2	4
3218.02	0.447	1.154	3217.97	0.311	0.545	Ne II	3218.19	V13	3p 4D*	3d 4F	8	10
			3231.14	0.042	0.074	He I	3231.26	N20	2s 1S	10p 1P*	1	3
			3244.19	0.199	0.346	Ne II	3244.09	V13	3p 4D*	3d 4F	6	8
			3296.79	0.075	0.127	He I	3296.77	V9	2s 1S	8p 1P*	1	3
			3297.75	0.041	0.069	Ne II	3397.72	V2	3s 4P	3p 4D*	6	6
3299.36	0.654	1.576	3299.39	0.155	0.260	O III	3299.36	V3	3s 3P*	3p 3S	1	3
3312.29	1.138	2.713	3312.32	0.465	0.777	O III	3312.30	V3	3s 3P*	3p 3S	3	3
			3320.86	0.058	0.097	Ne II	3320.20	V12	3p 4D*	3d 4D	8	6
			3323.76	0.107	0.178	Ne II	3323.74	V7	3s 2P	3p 2P*	4	4
			3327.14	0.037	0.061	Ne II	3327.15	V2	3s 4P	3p 4D*	4	4
			3329.40	0.079	0.131	Ne II	3329.16	V12	3p 4D*	3d 4D	8	8
3334.84	0.491	1.148	3334.87	0.357	0.590	Ne II	3334.84	V2	3s 4P	3p 4D*	6	8
3340.74	1.477	3.440	3340.77	0.592	0.977	O III	3340.74	V3	3s 3P*	3p 3S	5	3
			3342.61	0.080	0.133	[Ne III]	3342.42	F2	2p4 1D	2p4 1S	5	1
3355.02	0.358	0.824	3355.05	0.241	0.395	Ne II	3355.02	V2	3s 4P	3p 4D*	4	6
						He I	3354.55	V8	2s 1S	7p 1P*	1	3
			3360.33	0.049	0.080	Ne II	3360.60	V2	3s 4P	3p 4D*	2	4
			3367.17	0.086	0.140	Ne II	3367.22	V20	3p 2D*	3d 2F	6	8
						Ne II	3366.98	V12	3p 4D*	3d 4D	6	8
			3378.01	0.030	0.048	Ne II	3378.22	V7	3s 2P	3p 2P*	2	2
			3386.22	0.014	0.023	Ne II	3386.20	V12	3p 4D*	3d 4D	4	6
			3388.76	0.055	0.088	Ne II	3388.42	V20	3p 2D*	3d 2F	4	6
			3405.74	0.036	0.057	O III	3405.74	V15	3p 3P	3d 3P*	1	3
			3408.27	0.038	0.061	O III	3408.14	V15	3p 3P	3d 3P*	3	1
			3415.22	0.079	0.127	O III	3415.29	V15	3p 3P	3d 3P*	3	3
3417.70	0.140	0.308	3417.68	0.101	0.161	Ne II	3416.91	V21	3p 2D*	3d 2D	6	6
						Ne II	3417.69	V19	3p 2D*	3d 4F	6	8
			3423.11	0.047	0.075							
3428.67	0.377	0.819	3428.64	0.278	0.440	O III	3428.65	V15	3p 3P	3d 3P*	3	5
3433.53	0.146	0.317										
			3435.05	0.060	0.095							
			3440.22	0.095	0.150							
3444.09	2.768	5.944	3444.11	1.383	2.174	O III	3444.07	V15	3p 3P	3d 3P*	5	5
			3447.63	0.124	0.195	He I	3447.59	V7	2s 1S	6p 1P*	1	3
			3453.32	0.038	0.060	Ne II	3453.07	V21	3p 2D*	3d 2D	4	4
			3465.90	0.063	0.098	He I	3465.94		2p 3P*	17d 3D	9	15
			3477.35	0.037	0.057	Ne II	3477.65	V21	3p 2D*	3d 2D	4	6
3478.88	0.172	0.359	3478.93	0.076	0.117	He I	3478.97	V43	2p 3P*	15d 3D	9	15
			3481.37	0.050	0.078	Ne II	3481.93	V6	3s 2P	3p 2S	4	2
			3486.07	0.028	0.043							
3487.64	0.240	0.499	3487.69	0.051	0.079	He I	3487.73	V42	2p 3P*	14d 3D	9	15
3498.57	0.118	0.243	3498.49	0.105	0.160	He I	3498.66	V40	2p 3P*	13d 3D	9	15
3506.28	0.102	0.209										
3512.43	0.100	0.205	3512.35	0.137	0.208	He I	3512.52	V38	2p 3P*	12d 3D	9	15
3530.41	0.197	0.397	3530.32	0.156	0.237	He I	3530.50	V36	2p 3P*	11d 3D	9	15
			3537.17	0.030	0.046							
3541.06	0.133	0.266										
3550.28	0.140	0.277										
3554.33	0.219	0.434	3554.34	0.197	0.295	He I	3554.42	V34	2p 3P*	10d 3D	9	15
3568.43	0.175	0.342	3568.41	0.061	0.090	Ne II	3568.50	V9	3s' 2D	3p' 2F*	6	8
			3573.79	0.038	0.057	Ne II	3574.18	V9	3s' 2D	3p' 2F*	6	6
3587.22	0.206	0.399	3587.16	0.257	0.379	He I	3587.28	V32	2p 3P*	9d 3D	9	15
			3611.62	0.042	0.062							
3613.57	0.247	0.469	3613.52	0.243	0.356	He I	3613.64	V6	2s 1S	5p 1P*	1	3
			3632.07	0.046	0.067	Ne II	3632.68	V33	3p 4S*	3d 2D	4	4
3634.18	0.322	0.603	3634.13	0.407	0.590	He I	3634.25	V28	2p 3P*	8d 3D	9	15
3671.40	0.283	0.516	3671.39	0.370	0.528	H 24	3671.48	H24	2p+ 2P*	24d+ 2D	8	*
3673.66	0.254	0.462	3673.65	0.394	0.562	H 23	3673.74	H23	2p+ 2P*	23d+ 2D	8	*

Table 2 – *continued*

λ_{obs}	M1-42 $F(\lambda)$	$I(\lambda)$	λ_{obs}	M2-36 $F(\lambda)$	$I(\lambda)$	Ion	λ_0	Mult	Lower term	Upper term	g_1	g_2
3676.28	0.346	0.629	3676.27	0.452	0.644	H 22	3676.36	H22	2p+ 2P*	22d+ 2D	8	*
3679.28	0.413	0.750	3679.27	0.493	0.702	H 21	3679.36	H21	2p+ 2P*	21d+ 2D	8	*
3682.73	0.449	0.814	3682.71	0.540	0.768	H 20	3682.81	H20	2p+ 2P*	20d+ 2D	8	*
3686.75	0.485	0.877	3686.73	0.617	0.876	H 19	3686.83	H19	2p+ 2P*	19d+ 2D	8	*
3691.48	0.519	0.935	3691.46	0.710	1.006	H 18	3691.56	H18	2p+ 2P*	18d+ 2D	8	*
3694.13	0.252	0.452	3694.11	0.325	0.460	Ne II	3694.21	V1	3s 4P	3p 4P*	6	6
3697.07	0.511	0.916	3697.05	0.798	1.129	H 17	3697.15	H17	2p+ 2P*	17d+ 2D	8	*
3703.98	0.984	1.758	3703.97	1.367	1.928	H 16	3703.86	H16	2p+ 2P*	16d+ 2D	8	*
3705.13	0.413	0.737	3705.13	0.333	0.470	He I	3705.02	V25	2p 3P*	7d 3D	9	15
			3707.36	0.146	0.205	O III	3707.25	V14	3p 3P	3d 3D*	3	5
			3709.73	0.129	0.181	Ne II	3709.62	V1	3s 4P	3p 4P*	4	2
3712.09	1.190	2.115	3712.08	1.476	2.075	H 15	3711.97	H15	2p+ 2P*	15d+ 2D	8	*
3715.19	0.137	0.243				O III	3715.08	V14	3p 3P	3d 3D*	5	7
3722.05	2.230	3.938	3721.84	2.803	3.925	H 14	3721.94	H14	2p+ 2P*	14d+ 2D	8	*
*	*	*	*	*	*	[S III]	3721.63	F2	3p2 3P	3p2 1S	3	1
3725.93	19.54	34.42	3725.93	28.27	39.52	[O II]	3726.03	F1	2p3 4S*	2p3 2D*	4	4
3728.72	13.87	24.38	3728.72	14.37	20.07	[O II]	3728.82	F1	2p3 4S*	2p3 2D*	4	6
3734.33	1.323	2.317	3734.27	1.698	2.366	H 13	3734.37	H13	2p+ 2P*	13d+ 2D	8	*
			3739.82	0.064	0.089	O II	3739.76	V31	3p 4S*	4s 4P	4	6
3750.05	1.871	3.244	3750.05	2.384	3.303	H 12	3750.15	12	2p+ 2P*	12d+ 2D	8	*
3754.78	0.212	0.366	3754.60	0.185	0.255	O III	3754.69	V2	3s 3P*	3p 3D	3	5
3757.33	0.185	0.319	3757.15	0.107	0.147	O III	3757.24	V2	3s 3P*	3p 3D	1	3
3759.96	0.646	1.113	3759.77	0.347	0.479	O III	3759.87	V2	3s 3P*	3p 3D	5	7
			3761.97	0.062	0.085	O II	3762.46	V31	3p 4S*	4s 4P	4	4
			3766.64	0.112	0.154	Ne II	3766.26	V1	3s 4P	3p 4P*	4	6
3770.62	2.174	3.721	3770.61	2.759	3.793	H 11	3770.63	H11	2p+ 2P*	11d+ 2D	8	*
			3773.89	0.063	0.087	O III	3774.02	V2	3s 3P*	3p 3D	3	3
3777.14	0.068	0.116	3777.01	0.064	0.087	Ne II	3777.14	V1	3s 4P	3p 4P*	2	4
						O II	3777.42	V31	3p 4S*	4s 4P	4	2
3785.90	0.039	0.066	3784.53	0.023	0.031	He I	3784.89	V64	2p 1P*	12d 1D	3	5
3791.40	0.051	0.086	3791.14	0.042	0.058	O III	3791.27	V2	3s 3P*	3p 3D	5	5
3796.11	0.214	0.360	3796.12	0.293	0.399	Si III	3796.11	V5	4p 3P*	4d 3D	3	3
3797.90	2.711	4.560	3797.90	3.421	4.655	H 10	3797.90	H10	2p+ 2P*	10d+ 2D	8	*
3806.29	0.023	0.038	3805.66	0.030	0.040	He I	3805.76	V63	2p 1P*	11d 1D	3	5
3806.60	0.030	0.050	3806.46	0.031	0.042	Si III	3806.54	V5	4p 3P*	4d 3D	5	7
3813.56	0.085	0.142				He II	3813.50	4.19	4f+ 2F*	19g+ 2G	32	*
3819.68	1.040	1.726	3819.65	1.107	1.494	He I	3819.62	V22	2p 3P*	6d 3D	9	15
3833.42	0.301	0.495	3833.57	0.420	0.564	He I	3833.57	V62	2p 1P*	10d 1D	3	5
3835.44	4.461	7.332	3835.42	5.029	6.749	H 9	3835.39	H9	2p+ 2P*	9d+ 2D	8	*
3842.68	0.072	0.117				O II	3842.81	V12	3p 4D*	3d 4D	2	4
			3850.93	0.024	0.032	O II	3851.03	V12	3p 4D*	3d 4D	4	4
3856.11	0.161	0.261	3856.23	0.130	0.172	O II	3856.13	V12	3p 4D*	3d 4D	4	2
*	*	*	*	*	*	Si II	3856.02	V1	3p2 2D	4p 2P*	6	4
3858.05	0.187	0.303				He II	3858.07	4.17	4f+ 2F*	15g+ 2G	32	*
			3862.70	0.205	0.272	Si II	3862.60	V1	3p2 2D	4p 2P*	4	2
3868.79	41.71	67.17	3868.80	57.42	76.14	[Ne III]	3868.75	F1	2p4 3P	2p4 1D	5	5
			3882.38	0.140	0.184	O II	3882.19	V12	3p 4D*	3d 4D	8	8
3882.59	0.150	0.240				O II	3882.45	V11	3p 4D*	3d 4P	4	4
*	*	*	*	*	*	O II	3883.13	V12	3p 4D*	3d 4D	8	6
3888.86	14.09	22.42	3888.89	14.790	19.470	H 8	3889.05	H8	2p+ 2P*	8d+ 2D	8	*
						He I	3888.65	V2	2s 3S	3p 3P*	3	9
			3907.57	0.026	0.034	O II	3907.46	V11	3p 4D*	3d 4P	6	6
3912.28	0.048	0.076	3911.68	0.009	0.012	O II	3911.96	V17	3s' 2D	3p' 2P*	6	4
						O II	3912.11	V17	3s' 2D	3p' 2P*	4	4
3918.88	0.023	0.036	3919.09	0.020	0.026	C II	3918.98	V4	3p 2P*	4s 2S	2	2
3920.59	0.034	0.053	3920.80	0.036	0.047	C II	3920.69	V4	3p 2P*	4s 2S	4	2
3923.38	0.064	0.100	3923.59	0.028	0.037	He II	3923.48	4.15	4f+ 2F*	15g+ 2G	32	*
3926.44	0.076	0.118	3926.65	0.117	0.152	He I	3926.54	V58	2p 1P*	8d 1D	3	5
			3954.30	0.027	0.035	O II	3954.36	V6	3s 2P	3p 2P*	2	2
3964.79	1.011	1.536	3964.75	0.989	1.256	He I	3964.73	V5	2s 1S	4p 1P	1	3
3967.52	12.96	19.69	3967.48	9.57[a]	12.27[a]	[Ne III]	3967.46	F1	2p4 3P	2p4 1D	3	5
3970.13	6.629[a]	10.06[a]	3970.09	12.15	15.55	H 7	3970.07	H7	2p+ 2P*	7d+ 2D	8	98
3995.00	0.148	0.221	3995.03	0.034	0.043	N II	3994.99	V12	3s 1P*	3p 1D	3	5
3998.64	0.062	0.093	3998.67	0.017	0.022	N III	3998.63	V17	4d 2D	5f 2F*	4	6
4003.49	0.072	0.108	4003.62	0.016	0.020	N III	4003.58	V17	4d 2D	5f 2F*	6	8
4009.17	0.240	0.357	4009.30	0.193	0.244	He I	4009.26	V55	2p 1P*	7d 1D	3	5
4026.16	2.429	3.570	4026.19	2.511	3.154	He I	4026.21	V18	2p 3P*	5d 3D	9	15
*	*	*	*	*	*	N II	4026.08	V39b	3d 3F*	4f 2[5]	7	9
4035.03	0.202	0.295	4035.05	0.100	0.125	N II	4035.08	V39a	3d 3F*	4f 2[4]	5	7
4041.25	0.466	0.680	4041.28	0.180	0.225	N II	4041.31	V39b	3d 3F*	4f 2[5]	9	11

Table 2 – *continued*

λ_{obs}	M1-42 $F(\lambda)$	$I(\lambda)$	λ_{obs}	M2-36 $F(\lambda)$	$I(\lambda)$	Ion	λ_0	Mult	Lower term	Upper term	g_1	g_2
4043.47	0.179	0.261	4043.51	0.073	0.091	N II	4043.53	V39a	3d 3F*	4f 2[4]	7	9
			4048.18	0.012	0.015	O II	4048.21	V50b	3d 4F	4f F3*	8	8
			4060.77	0.022	0.027	O II	4060.01	V97	3d' 2F	4f' G4*	14	18
4063.01	0.106	0.152	4062.91	0.039	0.048	O II	4062.94	V50a	3d 4F	4f F4*	10	10
4068.61	1.651	2.373	4068.47	2.472	3.063	[S II]	4068.60	F1	2p3 4S*	2p3 2P*	4	4
4069.90	0.940	1.348	4069.49	0.980	1.213	O II	4069.89	V10	3p 4D*	3d 4F	4	6
4071.25	0.071	0.101	4071.10	0.061	0.075	O II	4071.23	V48a	3d 4F	4f G5*	8	10
4072.18	0.904	1.296	4072.06	0.778	0.963	O II	4072.16	V10	3p 4D*	3d 4F	6	8
4075.88	0.948	1.355	4075.73	0.898	1.110	O II	4075.86	V10	3p 4D*	3d 4F	8	10
4076.11	0.556	0.796	4076.22	0.833	1.030	[S II]	4076.35	F1	2p3 4S*	2p3 2P*	2	4
4078.86	0.151	0.215	4078.72	0.119	0.147	O II	4078.84	V10	3p 4D*	3d 4F	4	4
4083.74	0.209	0.298	4083.80	0.163	0.201	O II	4083.90	V48b	3d 4F	4f G4*	6	8
4084.95	0.160	0.228	4085.01	0.132	0.162	O II	4085.11	V10	3p 4D*	3d 4F	6	6
4086.99	0.206	0.293	4087.05	0.160	0.197	O II	4087.15	V48c	3d 4F	4f G3*	4	6
4089.13	0.560	0.796	4089.19	0.414	0.510	O II	4089.29	V48a	3d 4F	4f G5*	10	12
4092.76	0.140	0.199	4092.87	0.114	0.140	O II	4092.93	V10	3p 4D*	3d 4F	8	8
4097.24	2.359	3.336	4097.27	1.665	2.044	N III	4097.33	V1	3s 2S	3p 2P*	2	4
*	*	*	*	*	*	O II	4097.25	V20	3p 4P*	3d 4D	2	4
*	*	*	*	*	*	O II	4097.26	V48b	3d 4F	4f G4*	8	10
*	*	*	*	*	*	O II	4098.24	V46a	3d 4F	4f D3*	4	6
4101.66	18.05	25.44	4101.64	21.05	25.81	H 6	4101.74	H6	2p+ 2P*	6d+ 2D	8	72
4110.76	0.086	0.120	4110.80	0.077	0.094	O II	4110.78	V20	3p 4P*	3d 4D	4	2
4119.20	0.351	0.491	4119.06	0.297	0.362	O II	4119.22	V20	3p 4P*	3d 4D	6	8
4120.26	0.031	0.044	4120.12	0.027	0.032	O II	4120.28	V20	3p 4P*	3d 4D	6	6
4120.52	0.076	0.106	4120.38	0.064	0.078	O II	4120.54	V20	3p 4P*	3d 4D	6	4
4120.82	0.097	0.136	4120.68	0.154	0.188	He I	4120.84	V16	2p 3P*	5s 3S	9	3
4121.44	0.111	0.155	4121.31	0.094	0.115	O II	4121.46	V19	3p 4P*	3d 4P	2	2
			4128.17	0.031	0.038	Si II	4128.07	V3	3d 2D	4f 2F*	4	6
4129.24	0.041	0.057	4129.32	0.023	0.028	O II	4129.32	V19	3p 4P*	3d 4P	4	2
			4131.23	0.052	0.064	Si II	4030.89	V3	3d 2D	4f 2F*	6	8
4132.72	0.168	0.233	4132.80	0.149	0.180	O II	4132.80	V19	3p 4P*	3d 4P	2	4
4143.68	0.351	0.484	4143.75	0.386	0.469	He I	4143.76	V53	2p 1P*	6d 1D	3	5
4153.24	0.300	0.412	4153.18	0.235	0.283	O II	4153.30	V19	3p 4P*	3d 4P	4	6
4156.47	0.104	0.143	4156.41	0.118	0.142	O II	4156.53	V19	3p 4P*	3d 4P	6	4
4169.16	0.108	0.146	4169.10	0.111	0.134	O II	4169.22	V19	3p 4P*	3d 4P	6	6
*	*	*	*	*	*	He I	4168.97	V52	2p 1P*	6s 1S	3	1
4171.56	0.069	0.094	4171.38	0.028	0.033	N II	4171.61	V43a	3d 1D*	4f 1[4]	5	7
4176.09	0.135	0.183	4176.04	0.049	0.058	N II	4176.16	V43a	3d 1D*	4f 1[3]	5	7
4179.60	0.052	0.071	4179.55	0.019	0.023	N II	4179.67	V50a	3d 3D*	4f 2[3]	7	7
4185.38	0.056	0.076	4185.35	0.065	0.077	O II	4185.45	V36	3p' 2F*	3d' 2G	6	8
4186.83	0.035	0.047	4186.72	0.058	0.070	C III	4186.90	V18	4f 1F*	5g 1G	7	9
4189.72	0.045	0.060	4189.61	0.084	0.100	O II	4189.79	V36	3p' 2F*	3d' 2G	8	10
4195.69	0.041	0.055	4195.68	0.030	0.036	N III	4195.76	V6	3s' 2P*	3p' 2D	2	4
4199.76	0.168	0.226	4199.88	0.112	0.132	He II	4199.83	4.11	4f+ 2F*	11g+ 2G	32	*
4200.03	0.074	0.100				N III	4200.10	V6	3s' 2P*	3p' 2D	4	6
4219.73	0.135	0.178	4219.81	0.106	0.125	Ne II	4219.74	V52a	3d 4D	4f 2[4]*	8	10
*	*	*	*	*	*	Ne II	4219.37	V52a	3d 4D	4f 2[4]*	8	8
			4231.56	0.039	0.046	Ne II	4231.64	V52b	3d 4D	4f 2[3]*	6	*
*	*	*	*	*	*	Ne II	4231.53	V52b	3d 4D	4f 2[3]*	6	6
4233.84	0.024	0.032	4233.78	0.027	0.032	Ne II	4233.85	V52a	3d 4D	4f 2[4]*	6	*
4236.90	0.128	0.169	4236.84	0.052	0.061	N II	4236.91	V48a	3d 3D*	4f 1[3]	3	5
4237.04	0.190	0.250	4236.98	0.077	0.090	N II	4237.05	V48b	3d 3D*	4f 1[4]	5	7
4241.23	0.039	0.051	4241.17	0.015	0.017	N II	4241.24	V48a	3d 3D*	4f 1[3]	5	5
4241.77	0.523	0.685	4241.71	0.170	0.199	N II	4241.78	V48b	3d 3D*	4f 1[4]	7	9
			4250.50	0.025	0.029	Ne II	4250.65	V52b	3d 4D	4f 2[3]*	4	6
			4253.85	0.067	0.079	O II	4254.00	V101	3d' 2G	4f' H5*	18	22
			4257.91	0.020	0.023	Ne II	4257.80	V52d	3d 4D	4f 2[2]*	2	4
4267.09	1.968	2.551	4267.12	2.121	2.471	C II	4267.15	V6	3d 2D	4f 2F*	10	14
4273.03	0.030	0.038	4273.04	0.022	0.025	O II	4273.10	V67a	3d 4D	4f F4*	6	8
4274.17	0.013	0.016	4274.18	0.009	0.011	O II	4274.24	v67a	3d 4D	4f F4*	8	8
4275.48	0.312	0.403	4275.49	0.231	0.269	O II	4275.55	V67a	3d 4D	4f F4*	8	10
4275.92	0.060	0.077	4275.93	0.044	0.052	O II	4275.99	V67b	3d 4D	4f F3*	4	6
4276.21	0.043	0.056	4276.22	0.032	0.037	O II	4276.28	V67b	3d 4D	4f F3*	6	6
4276.55	0.018	0.024	4276.56	0.014	0.016	O II	4276.62	V53c	3d 4D	4f D1*	4	4
4276.68	0.115	0.149	4276.69	0.085	0.099	O II	4276.75	V67b	3d 4D	4f F3*	6	8
4277.36	0.077	0.099	4277.37	0.057	0.066	O II	4277.43	V67c	3d 4D	4f F2*	2	4
4277.82	0.057	0.073	4277.83	0.042	0.049	O II	4277.89	V67b	3d 4D	4f F3*	8	8
4281.43	0.052	0.067	4281.25	0.027	0.032	O II	4281.32	V53b	3d 4P	4f D2*	6	6
4283.07	0.087	0.112	4282.89	0.089	0.104	O II	4282.96	V67c	3d 4D	4f F2*	4	6
4283.84	0.095	0.122	4283.66	0.051	0.059	O II	4283.73	V67c	3d 4D	4f F2*	4	4

Table 2 – *continued*

λ_{obs}	M1-42 $F(\lambda)$	$I(\lambda)$	λ_{obs}	M2-36 $F(\lambda)$	$I(\lambda)$	Ion	λ_0	Mult	Lower term	Upper term	g_1	g_2
4285.80	0.102	0.132	4285.62	0.090	0.104	O II	4285.69	V78b	3d 2F	4f F3*	6	8
4288.71	0.079	0.101	4288.74	0.028	0.033	O II	4288.82	V53c	3d 4P	4f D1*	2	4
*	*	*	*	*	*	O II	4288.82	V53c	3d 4P	4f D1*	2	2
4291.14	0.128	0.163	4291.17	0.068	0.079	O II	4291.25	V55	3d 4P	4f G3*	6	8
4292.10	0.050	0.064	4292.13	0.061	0.071	O II	4292.21	V78c	3d 2F	4f F2*	6	6
4294.67	0.130	0.166	4294.71	0.099	0.114	O II	4294.78	V53b	3d 4P	4f D2*	4	6
4294.81	0.031	0.039	4294.85	0.023	0.027	O II	4294.92	V53b	3d 4P	4f D2*	4	4
4303.56	0.050	0.064				O II	4303.61	V65a	3d 4D	4f G5*	8	10
4303.77	0.368	0.467	4303.71	0.254	0.293	O II	4303.82	V53a	3d 4P	4f D3*	6	8
4307.18	0.078	0.099	4307.12	0.045	0.052	O II	4307.23	V53b	3d 4P	4f D2*	2	4
			4308.81	0.040	0.046							
4312.06	0.049	0.063	4312.06	0.030	0.035	O II	4312.11	V78a	3d 2F	4f F4*	8	8
4313.39	0.086	0.108	4313.39	0.051	0.059	O II	4313.44	V78a	3d 2F	4f F4*	8	10
4315.34	0.089	0.112	4315.34	0.055	0.064	O II	4315.40	V63c	3d 4D	4f D1*	4	4
						O II	4315.39	V63c	3d 4D	4f D1*	4	2
*	*	*	*	*	*	O II	4315.39	V63c	3d 4D	4f D1*	4	2
*	*	*	*	*	*	O II	4315.83	V78b	3d 2F	4f F3*	8	8
4317.09	0.185	0.233	4317.09	0.166	0.191	O II	4317.14	V2	3s 4P	3p 4P*	2	4
4317.65	0.081	0.103	4317.65	0.032	0.036	O II	4317.70	V53a	3d 4P	4f D3*	4	6
4319.58	0.166	0.209	4319.58	0.119	0.136	O II	4319.63	V2	3s 4P	3p 4P*	4	6
4325.71	0.029	0.036	4325.71	0.042	0.048	O II	4325.76	V2	3s 4P	3p 4P*	2	2
4331.08	0.066	0.083	4331.08	0.046	0.052	O II	4331.13	V65b	3d 4D	4f G4*	6	8
4332.66	0.082	0.103	4332.67	0.063	0.072	O II	4332.71	V65b	3d 4D	4f G4*	8	10
4334.15	0.087	0.109	4334.15	0.042	0.047	O II	4334.19	V63b	3d 4D	4f D2*	6	6
4340.34	36.27	45.31	4340.39	41.54	47.40	H 5	4340.47	H5	2p+ 2P*	5d+ 2D	8	50
4345.44	0.356	0.444	4345.45	0.259	0.295	O II	4345.56	V2	3s 4P	3p 4P*	4	2
*	*	*	*	*	*	O II	4345.55	V65c	3d 4D	4f G3*	8	8
4349.30	0.447	0.556	4349.32	0.343	0.390	O II	4349.43	V2	3s 4P	3p 4P*	6	6
4353.46	0.075	0.093	4353.48	0.048	0.055	O II	4353.59	V76c	3d 2F	4f G3*	6	8
4357.12	0.069	0.085	4357.15	0.050	0.057	O II	4357.25	V63a	3d 4D*	4f D3*	6	8
	*	*	*	*	*	O II	4357.25	V63a	3d 4D*	4f D3*	6	6
4363.17	2.015	2.493	4363.12	2.409	2.731	[O III]	4363.21	F2	2p2 1D	2p2 1S	5	1
4366.84	0.292	0.360	4366.74	0.229	0.260	O II	4366.89	V2	3s 4P	3p 4P*	6	4
4369.81	0.078	0.096				Ne II	4369.86	V56	3d 4F	4f 0[3]*	4	6
4371.57	0.066	0.082	4371.47	0.081	0.091	O II	4371.62	V76b	3d 2F	4f G4*	8	10
4377.17	0.110	0.135	4377.15	0.043	0.049							
4379.08	0.979	1.202	4379.05	0.390	0.441	N III	4379.11	V18	4f 2F*	5g 2G	14	18
*	*	*	*	*	*	Ne II	4379.55	V60b	3d 2F	4f 1[4]*	8	10
4385.91	0.032	0.039	4385.96	0.058	0.065	O II	4386.01		3d' 2D	4f' G4*	6	8
4387.84	0.640	0.782	4387.88	0.609	0.686	He I	4387.93	V51	2p 1P*	5d 1D	3	5
4391.91	0.147	0.179	4391.85	0.131	0.148	Ne II	4391.99	V55e	3d 4F	4f 2[5]*	10	12
*	*	*	*	*	*	Ne II	4392.00	V55e	3d 4F	4f 2[5]*	10	10
4397.90	0.027	0.033	4397.85	0.046	0.051	Ne II	4397.99	V57b	3d 4F	4f 1[4]*	6	8
4409.06	0.129	0.156	4409.16	0.114	0.127	Ne II	4409.30	V55e	3d 4F	4	*	*
4413.27	0.089	0.107	4413.08	0.061	0.068	Ne II	4413.22	V65	3d 4P	4	*	*
*	*	*	*	*	*	Ne II	4413.11	V57c	3d 4F	4f 1[3]*	4	6
*	*	*	*	*	*	Ne II	4413.11	V65	3d 4P	4f 0[3]*	6	6
4414.92	0.186	0.225	4414.75	0.148	0.166	O II	4414.90	V5	3s 2P	3p 2D*	4	6
4416.81	0.156	0.188	4416.83	0.124	0.139	O II	4416.97	V5	3s 2P	3p 2D*	2	4
4427.52	0.116	0.139	4427.13	0.033	0.037	Ne II	4427.11	V55b	3d 4F	4f 2[3]*	8	6
						N II	4427.24	V55b	3d 3P*	4f 2[2]	3	5
						N II	4427.86	V55b	3d 3P*	4f 2[2]	3	3
4428.72	0.073	0.088	4428.54	0.079	0.088	Ne II	4428.64	V60c	3d 2F	4f 1[3]*	6	8
*	*	*	*	*	*	Ne II	4428.52	V61b	3d 2D	4f 2[3]*	6	8
4430.95	0.107	0.128	4430.84	0.063	0.071	Ne II	4430.94	V61a	3d 2D	4f 2[4]*	6	8
4432.75	0.305	0.366	4432.64	0.075	0.084	N II	4432.74	V55a	3d 3P*	4f 2[3]	5	7
			4433.38	0.029	0.032	N II	4433.48	V55b	3d 3P*	4f 2[2]	1	3
4437.61	0.041	0.049	4437.45	0.062	0.069	He I	4437.55	V50	2p 1P*	5s 1S	3	1
4442.10	0.073	0.087	4441.95	0.023	0.026	N II	4442.02	V55a	3d 3P*	4f 2[3]	3	5
4448.25	0.074	0.088	4448.12	0.017	0.018	O II	4448.19	V35	3p' 2F*	3d' 2F	8	8
4452.89	0.036	0.042	4452.30	0.020	0.022	O II	4452.37	V5	3s 2P	3p 2D*	4	4
4457.27	0.054	0.065	4456.98	0.036	0.040	Ne II	4457.05	V61a	3d 2D	4f 2[4]*	6	8
*	*	*	*	*	*	Ne II	4457.24	V61d	3d 2D	4f 2[2]*	4	4
4464.48	0.069	0.082	4464.98	0.036	0.040							
4466.48	0.087	0.103	4466.35	0.060	0.066	O II	4466.42	V86b	3d 2P	4f D2*	4	6
4471.36	6.186	7.280	4471.37	6.064	6.675	He I	4471.50	V14	2p 3P*	4d 3D	9	15
4477.91	0.066	0.078	4477.87	0.050	0.055	O II	4477.90	V88	3d 2P	4f G3*	4	6
4481.22	0.055	0.064	4481.18	0.043	0.047	Mg II	4481.21	V4	3d 2D	4f 2F*	10	14
			4482.81	0.020	0.022							
4487.73	0.056	0.066	4487.69	0.034	0.037	O II	4487.72	V104	3d' 2P	4f' D2*	2	4

Table 2 – *continued*

λ_{obs}	M1-42 $F(\lambda)$	$I(\lambda)$	λ_{obs}	M2-36 $F(\lambda)$	$I(\lambda)$	Ion	λ_0	Mult	Lower term	Upper term	g_1	g_2
4489.51	0.050	0.059	4489.46	0.034	0.038	O II	4489.49	V86b	3d 2P	4f D2*	2	4
4491.09	0.075	0.088	4491.04	0.042	0.046	C II	4491.07		4f 2F*	9g 2G	14	18
4491.25	0.105	0.123	4491.21	0.062	0.068	O II	4491.23	V86a	3d 2P	4f D3*	4	6
4499.04	0.046	0.053	4499.10	0.024	0.026	Ne II	4499.12	V64c	3d 4P	4f 2[1]*	2	2
						Ne II	4498.92	V64c	3d 4P	4f 2[1]*	2	4
4508.38	0.082	0.095	4507.96	0.029	0.032							
4510.89	0.299	0.345	4510.72	0.160	0.175	N III	4510.91	V3	3s' 4P*	3p' 4D	4	6
*	*	*	*	*	*	N III	4510.91	V3	3s' 4P*	3p' 4D	2	4
4514.74	0.063	0.072	4514.68	0.038	0.042	N III	4514.86	V3	3s' 4P*	3p' 4D	6	8
4518.03	0.070	0.080	4517.96	0.054	0.059	N III	4518.15	V3	3s' 4P*	3p' 4D	2	2
4523.46	0.113	0.130	4523.40	0.069	0.075	N III	4523.58	V3	3s' 4P*	3p' 4D	4	4
4530.32	0.260	0.298	4530.41	0.108	0.117	N II	4530.41	V58b	3d 1F*	4f 2[5]	7	9
*	*	*	*	*	*	N III	4530.86	V3	3s' 4P*	3p' 4D	4	2
4534.49	0.062	0.071	4534.58	0.053	0.057	N III	4534.58	V3	3s' 4P*	3p' 4D	6	6
4539.62	0.071	0.081	4539.71	0.026	0.028	N III	4539.71	V12	4p 2P*	5s 2S	2	2
4541.50	0.339	0.387	4541.58	0.089	0.096	He II	4541.59	4.9	4f+ 2F*	9g+ 2G	32	*
4544.76	0.033	0.038	4544.84	0.032	0.034	N III	4544.85	V12	4p 2P*	5s 2S	4	2
4552.44	0.137	0.155	4552.46	0.063	0.068	N II	4552.53	V58a	3d 1F*	4f 2[4]	7	9
4562.51	0.126	0.143	4562.59	0.036	0.038	Mg I]	4562.60		3s2 1S	3s3p 3P*	1	5
4568.96	0.056	0.063	4569.04	0.039	0.041	Ne II	4569.05	V69b	3d 2P	4f 1[3]*	4	6
4571.01	0.136	0.153	4571.10	0.135	0.145	Mg I]	4571.10		3s2 1S	3s3p 3P*	1	3
4590.98	0.110	0.122	4590.83	0.122	0.130	O II	4590.97	V15	3s' 2D	3p' 2F*	6	8
			4596.04	0.074	0.079	O II	4596.18	V15	3s' 2D	3p' 2F*	4	6
*	*	*	*	*	*	O II	4595.96	V15	3s' 2D	3p' 2F*	6	6
4601.38	0.133	0.147	4601.34	0.032	0.034	N II	4601.48	V5	3s 3P*	3p 3P	3	5
4602.03	0.177	0.197	4601.99	0.089	0.094	O II	4602.13	V92b	3d 2D	4f F3*	4	6
4607.06	0.097	0.107	4606.99	0.048	0.052	N II	4607.16	V5	3s 3P*	3p 3P	1	3
4609.34	0.365	0.404	4609.27	0.196	0.208	O II	4609.44	V92a	3d 2D	4f F4*	6	8
4610.10	0.074	0.082	4610.03	0.088	0.093	O II	4610.20	V92c	3d 2D	4f F2*	4	6
4613.49	0.130	0.143	4613.52	0.062	0.066	O II	4613.68	V92b	3d 2D	4f F3*	6	8
						O II	4613.14	V92b	3d 2D	4f F3*	6	6
*	*	*	*	*	*	O II	4613.68	V92b	3d 2D	4f F3*	6	8
4621.29	0.153	0.169	4621.23	0.051	0.054	N II	4621.39	V5	3s 3P*	3p 3P	3	1
4630.46	0.396	0.435	4630.44	0.132	0.140	N II	4630.54	V5	3s 3P*	3p 3P	5	5
4634.06	1.204	1.320	4634.04	0.612	0.646	N III	4634.14	V2	3p 2P*	3d 2D	2	4
4638.79	0.634	0.693	4638.77	0.493	0.520	O II	4638.86	V1	3s 4P	3p 4D*	2	4
4640.57	2.565	2.803	4640.55	1.261	1.329	N III	4640.64	V2	3p 2P*	3d 2D	4	6
4641.74	1.049	1.146	4641.72	0.774	0.816	O II	4641.81	V1	3s 4P	3p 4D*	4	6
4641.77	0.241	0.263	4641.75	0.122	0.129	N III	4641.84	V2	3p 2P*	3d 2D	4	4
4643.01	0.182	0.199	4642.99	0.091	0.096	N II	4643.08	V5	3s 3P*	3p 3P	5	3
4647.38	0.127	0.139	4647.32	0.205	0.216	C III	4647.42	V1	3s 3S	3p 3P*	3	5
4649.09	1.619	1.763	4649.03	1.289	1.355	O II	4649.13	V1	3s 4P	3p 4D*	6	8
4650.21	0.076	0.083	4650.15	0.123	0.129	C III	4650.25	V1	3s 3S	3p 3P*	3	3
4650.80	0.491	0.534	4650.74	0.353	0.371	O II	4650.84	V1	3s 4P	3p 4D*	2	2
4651.43	0.040	0.044	4651.37	0.034	0.036	C III	4651.47	V1	3s 3S	3p 3P*	3	1
4654.24	0.045	0.049				Si IV	4654.32	V7	5g 2G	6h 2H*	18	22
			4658.02	0.047	0.049	[Fe III]	4658.10	F3	3d6 5D	3d6 3F2	9	9
4661.63	0.573	0.620	4661.55	0.412	0.432	O II	4661.63	V1	3s 4P	3p 4D*	4	4
4669.27	0.043	0.047	4669.19	0.025	0.027	O II	4669.27	V89b	3d 2D	4f D2*	4	6
4673.73	0.122	0.132	4673.65	0.078	0.081	O II	4673.73	V1	3s 4P	3p 4D*	4	2
4676.25	0.406	0.437	4676.16	0.299	0.312	O II	4676.24	V1	3s 4P	3p 4D*	6	6
4678.15	0.072	0.077	4678.06	0.036	0.038	N II	4678.14	V61b	3d 1P*	4f 2[2]	3	5
4685.71	12.56	13.46	4685.66	3.294	3.433	He II	4685.68	3.4	3d+ 2D	4f+ 2F*	18	32
			4693.46	0.018	0.019	O II	4693.20		3d 2D	4f G3*	6	6
4694.71	0.106	0.113	4694.78	0.029	0.030	N II	4694.64	V61a	3d 1P*	4f 2[3]	3	5
4696.45	0.063	0.067	4696.34	0.045	0.047	O II	4696.35	V1	3s 4P	3p 4D*	6	4
4699.56	0.050	0.054	4699.21	0.040	0.042	O II	4699.22	V25	3p 2D*	3d 2F	4	6
4705.69	0.097	0.103	4705.34	0.023	0.024	O II	4705.35	V25	3p 2D*	3d 2F	6	8
4711.39	1.709	1.814	4711.33	1.416	1.467	[Ar IV]	4711.37	F1	3p3 4S*	3p3 2D*	4	6
4713.19	0.606	0.642	4713.13	0.700	0.725	He I	4713.17	V12	2p 3P*	4s 3S	9	3
4724.28	0.028	0.030				[Ne IV]	4724.15	F1	2p3 2D*	2p3 2P*	4	4
4725.75	0.034	0.035				[Ne IV]	4725.62	F1	2p3 2D*	2p3 2P*	4	2
4740.28	1.316	1.381	4740.20	1.589	1.634	[Ar IV]	4740.17	F1	3p3 4S*	3p3 2D*	4	4
4774.40	0.046	0.048				N II	4774.24	V20	3p 3D	3d 3D*	3	5
4779.83	0.082	0.085	4779.12	0.014	0.014	N II	4779.72	V20	3p 3D	3d 3D*	3	3
4788.24	0.127	0.131	4788.02	0.029	0.030	N II	4788.13	V20	3p 3D	3d 3D*	5	5
			4802.12	0.036	0.037	C II	4802.23		4f 2F*	8g 2G	14	18
4803.36	0.311	0.318	4803.18	0.097	0.098	N II	4803.29	V20	3p 3D	3d 3D*	7	7
4815.61	0.092	0.093	4815.44	0.040	0.040	S II	4815.55	V9	4s 4P	4p 4S*	6	4
4861.38	100.0	100.0	4861.56	100.0	100.0	H 4	4861.33	H4	2p+ 2p*	4d+ 2D	*	*

Table 2 – *continued*

λ_{obs}	M1-42 $F(\lambda)$	$I(\lambda)$	λ_{obs}	M2-36 $F(\lambda)$	$I(\lambda)$	Ion	λ_0	Mult	Lower term	Upper term	g_1	g_2
4891.04	0.044	0.044	4890.89	0.042	0.042	O II	4890.86	V28	3p 4S*	3d 4P	4	2
4907.02	0.164	0.161	4906.95	0.094	0.093	O II	4906.83	V28	3p 4S*	3d 4P	4	4
4922.04	1.942	1.899	4921.91	1.868	1.843	He I	4921.93	V48	2p 1P*	4d 1D	3	5
4924.64	0.291	0.284	4924.51	0.216	0.213	O II	4924.53	V28	3p 4S*	3d 4P	4	6
4931.22	0.131	0.128	4931.22	0.111	0.109	[O III]	4931.80	F1	2p2 3P	2p2 1D	1	5
			4940.49	0.029	0.029	O II	4941.07	V33	3p 2P*	3d 2D	2	4
4943.38	0.050	0.049	4942.83	0.041	0.040	O II	4943.00	V33	3p 2P*	3d 2D	4	6
4958.96	177.0	170.6	4958.73	271.5	264.2	[O III]	4958.91	1	p2 3P	2p2 1D	3	5
5006.72	544.4	515.4	5006.73	829.7	796.7	[O III]	5006.84	F1	2p2 3P	2p2 1D	5	5
5041.12	0.723	0.681	5041.37	0.437	0.420	Si II	5041.03	V5	4p 2P*	4d 2D	2	4
5047.83	0.340	0.317	5048.08	0.228	0.219	He I	5047.74	V47	2p 1P*	4s 1S	3	1
5056.08	0.343	0.320	5056.33	0.164	0.158	Si II	5055.98	V5	4p 2P*	4d 2D	4	6
*	*	*	*	*	*	Si II	5056.31	V5	4p 2P*	4d 2D	4	4
			5190.24	0.082	0.077	[Ar III]	5191.82	F3	2p4 1D	2p4 1S	5	1
5199.01	3.652	3.237	5198.27	1.067	0.994	[N I]	5199.84	F1	2p3 4S*	2p3 2D*	4	4
*	*	*	*	*	*	[N I]	5200.26	F1	2p3 4S*	2p3 2D*	4	6
5342.73	0.279	0.236	5342.11	0.138	0.125	C II	5342.38		4f 2F*	7g 2G	14	18
5377.46	0.515	0.431	5376.95	0.077	0.070							
5411.88	2.163	1.790	5411.24	0.325	0.290	He II	5411.52	4.7	4f+ 2F*	7g+ 2G	32	98
5518.03	0.808	0.648	5517.39	0.620	0.544	[Cl III]	5517.66	F1	2p3 4S*	2p3 2D*	4	6
5537.98	0.775	0.617	5537.32	0.876	0.766	[Cl III]	5537.60	F1	2p3 4S*	2p3 2D*	4	4
5577.72	0.429	0.338	5577.06	0.077	0.066	[O I]	5577.34	F3	2p4 1D	2p4 1S	5	1
5666.96	0.877	0.673	5666.55	0.220	0.188	N II	5666.63	V3	3s 3P*	3p 3D	3	5
5676.35	0.417	0.319	5675.94	0.091	0.078	N II	5676.02	V3	3s 3P*	3p 3D	1	3
5679.89	1.665	1.274	5679.49	0.455	0.388	N II	5679.56	V3	3s 3P*	3p 3D	5	7
5686.53	0.269	0.205	5686.14	0.088	0.075	N II	5686.21	V3	3s 3P*	3p 3D	3	3
5711.10	0.259	0.197	5710.69	0.106	0.090	N II	5710.77	V3	3s 3P*	3p 3D	5	5
5754.41	4.106	3.078	5754.52	2.424	2.042	[N II]	5754.60	F3	2p2 1D	2p2 1S	5	1
5875.60	32.79	23.80	5875.52	24.31	20.11	He I	5875.66	V11	2p 3p*	3d 3D	9	15
5931.89	0.323	0.231	5932.05	0.078	0.064	N II	5931.78	V28	3p 3P	3d 3D*	3	5
*	*	*	*	*	*	He II	5931.84	5.25	5g+ 2G	25h+ 2H*	50	*
5940.32	0.088	0.063	5940.49	0.024	0.019	N II	5940.24	V28	3p 3P	3d 3D*	3	3
5941.76	0.495	0.353	5941.92	0.133	0.109	N II	5941.65	V28	3p 3P	3d 3D*	5	7
6037.10	0.409	0.285										
			6073.82	0.102	0.082							
6076.42	0.371	0.256										
			6101.55	0.161	0.128	[K IV]	6101.83	F1	3p4 3P	3d4 1D	5	5
			6152.08	0.138	0.110	C II	6151.43	16.04	4d 2D	6f 2F*	10	14
6300.96	7.640	4.999	6300.65	8.832	6.871	[O I]	6300.34	F1	2p4 3P	2p4 1D	5	5
6312.73	2.202	1.437	6312.40	1.921	1.492	[S III]	6312.10	F3	2p2 1D	2p2 1S	5	1
*	*	*	*	*	*	He II	6310.80	5.16	5g+ 2G	16h+ 2H*	50	*
			6347.40	0.204	0.158	Si II	6347.10	V2	4s 2S	4p 2P*	2	4
6364.78	2.617	1.688	6364.08	2.984	2.302	[O I]	6363.78	F1	2p4 3P	2p4 1D	3	5
6372.33	0.553	0.356	6371.69	0.227	0.175	Si II	6371.38	V2	4s 2S	4p 2P*	2	2
			6461.96	0.317	0.241	C II	6461.95		4f 2F*	6g 2G	14	18
			6482.07	0.063	0.048	N II	6482.05	V8	3s 1P*	3p 1P	3	3
6548.86	143.7	89.05	6548.61	63.22	47.63	[N II]	6548.10	F1	2p2 3P	2p2 1D	3	5
6563.52	522.8	323.0	6563.65	419.9	315.7	H 3	6562.77	H3	2p+ 2p*	3d+ 2D	8	18
6584.30	449.0	276.2	6584.02	196.3	147.2	[N II]	6583.50	F1	2p2 3P	2p2 1D	5	5
6679.04	11.280	6.805	6678.68	8.054	5.972	He I	6678.16	V46	2p 1p*	3d 1D	3	5
6717.32	28.45	17.03	6716.97	12.14	8.96	[S II]	6716.44	F2	2p3 4S*	2p3 2D*	4	6
6731.71	34.62	20.67	6731.34	20.17	14.86	[S II]	6730.82	F2	2p3 4S*	2p3 2D*	4	4
7065.75	6.640	3.720	7065.79	8.157	5.789	He I	7065.25	V10	2p 3p*	3s 3S	9	3
7136.05	33.19	18.36	7136.34	26.82	18.89	[Ar III]	7135.80	F1	3p4 3p	3p4 1D	5	5
7177.58	0.467	0.256				He II	7177.50	5.11	5g+ 2G	11h+ 2H*	50	*
7182.71	0.257	0.141										
7231.55	1.025	0.558	7232.01	0.621	0.433	C II	7231.32	V3	3p 2P*	3d 2D	2	4
7236.73	1.690	0.919	7237.19	1.206	0.841	C II	7236.42	V3	3p 2P*	3d 2D	4	6
*	*	*	*	*	*	C II	7237.17	V3	3p 2P*	3d 2D	4	4
*	*	*	*	*	*	[Ar IV]	7237.26	F2	3p3 2D*	3p3 2P*	6	4
			7263.30	0.070	0.049	[Ar IV]	7262.76	F2	3p3 2D*	3p3 2P*	4	2
7281.22	1.541	0.831	7282.05	0.917	0.636	He I	7281.35	V45	2p 1P*	3s 1S	3	1
7319.03	4.426	2.372	7320.35	5.260	3.636	[O II]	7318.92	F2	2p3 2D*	2p3 2P*	6	2
*	*	*	*	*	*	[O II]	7319.99	F2	2p3 2D*	2p3 2P*	6	4
7329.59	3.811	2.039	7330.75	4.421	3.053	[O II]	7329.67	F2	2p3 2D*	2p3 2P*	4	2
*	*	*	*	*	*	[O II]	7330.73	F2	2p3 2D*	2p3 2P*	4	4

[a] Affected by the interstellar Ca II H line absorption.

Table 3. *ISO* SWS and LWS fluxes.

Line	$F(\lambda)$ (10^{-12} erg cm^{-2} s^{-1})		$I(\lambda)$ [$I(\mathrm{H}\beta) = 100$]	
	M 1-42	M 2-36	M 1-42	M 2-36
[Ar III] 9.0 μm	4.06	2.63	34.5	39.8
[S IV] 10.5 μm	11.3	18.9	96.2	286.
[Ne II] 15.6 μm	20.0	38.7	170.	586.
[S III] 18.7 μm	5.21	7.71	44.3	117.
[O IV] 25.9 μm	2.58	–	22.0	–
[S III] 33.5 μm	13.5	8.62	115.	130.
[Ne III] 36.0 μm	3.50	3.49	29.8	52.8
[O III] 52 μm	38.7	22.1	329.	334.
[N III] 57 μm	28.4	5.81	242.	87.9
[O I] 63 μm	2.90	1.98	24.7	30.0
[O III] 88 μm	18.7	7.28	159.	110.
[N II] 122 μm	.775		6.60	–

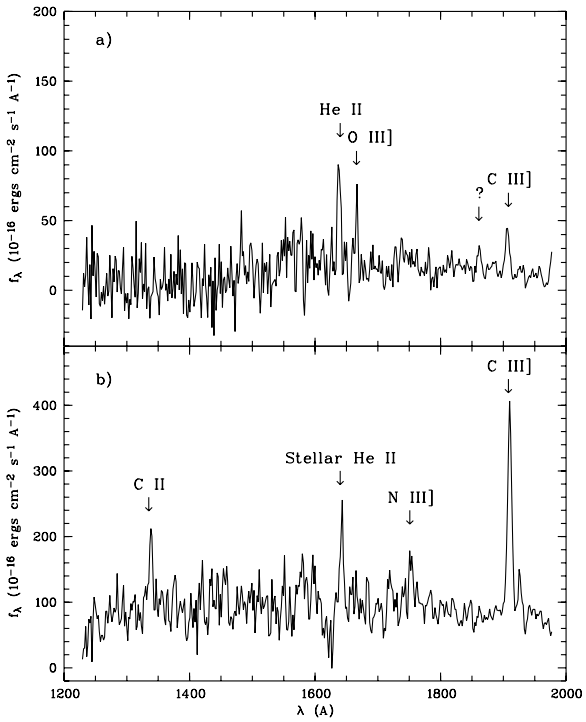

Figure 2. The *IUE* large aperture spectra of (a) M 1-42 and (b) M 2-36.

Similarly, for M 2-36 we find

$$A(\lambda) = -0.517 + 0.580x.$$

In terms of the normalized extinction, $X(x)$, both fits yield an identical result,

$$X(x) = -4.00 + 2.20x.$$

In nebular analyses, the reddening law is often presented in the form of $f(\lambda)$, with the total extinction at a given wavelength λ given by $10^{c[1+f(\lambda)]}$, where c is the logarithmic extinction at Hβ [i.e. for Hβ at 4861 Å, $f(\lambda 4861) = 0$]. We have, $A(\lambda) = 2.5c[1 + f(\lambda)]$ and $c = 0.4A(\mathrm{H}\beta)$. The fitted extinction curve towards M 1-42 given above then yields,

$$f(\lambda) = -1.15 + 0.56x, \quad (1)$$

Table 4. *IUE* fluxes.

Line	$F(\lambda)$ (10^{-14} erg cm^{-2} s^{-1})		$I(\lambda)$ [$I(\mathrm{H}\beta) = 100$]	
	M 1-42	M 2-36	M 1-42	M 2-36
C II λ1335	–	7.89	–	40.5
He II λ1640	4.87	Stellar	80.0	Stellar
N III] λ1751	–	6.46	–	12.8
O III] λ1664	1.94	–	29.2	–
Al III λ1863?	1.01	–	8.59	–
C III] λ1908	2.38	25.5	18.0	39.4

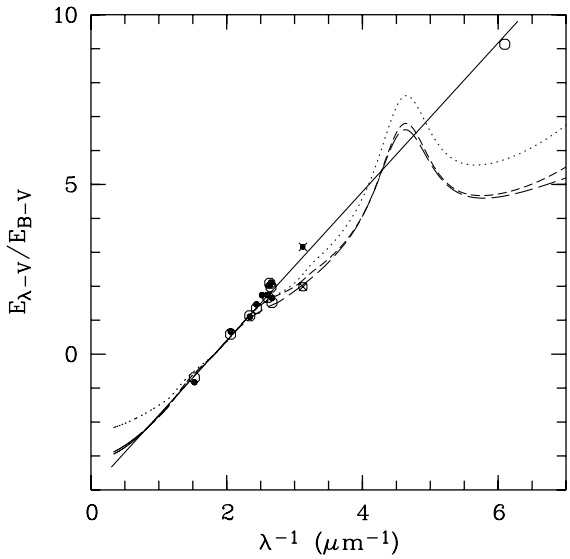

Figure 3. Normalized extinction towards M 1-42 (open circles) and M 2-36 (filled circles). The solid line represents straight line fits to the data points from M 1-42 and M 2-36, which yields nearly an identical result, $X(x) \equiv E(\lambda - V)/E(B - V) = -4.00 + 2.20x$, where $x = 1/\lambda\,\mu\mathrm{m}^{-1}$. The two data points with a cross are values derived from the He II λ3203 line and were excluded in the fitting. The long-dash curve is the Galactic standard reddening curve for $R = 3.1$ (Howarth 1983) and the short-dash and dotted lines are the R-dependent reddening curves from Cardelli et al. (1989) for $R = 3.1$ and 2.3, respectively.

and $c = 0.70$. Similarly for M 2-36, we have

$$f(\lambda) = -1.77 + 0.86x, \quad (2)$$

and $c = 0.27$.

The $f(\lambda)$ values calculated from the above two equations for M 1-42 and M 2-36 are tabulated in Table 2, along with dereddened line intensities (normalized such that $\mathrm{H}\beta = 100$), $I(\lambda) = 10^{cf(\lambda)}F(\lambda)$. The same equations were used to deredden the *IUE* fluxes listed in Table 4. After the extinction correction, the He II λ1640/λ4686 line ratio in M 1-42 is 5.94, compared to the predicted value of 5.65 for $T_\mathrm{e} = 4000$ K and $N_\mathrm{e} = 1100\,\mathrm{cm}^{-3}$.

4 PLASMA DIAGNOSTICS

The electron temperatures and densities derived from various CEL diagnostic ratios are presented in Table 6. For M 1-42 and M 2-36, the electron temperatures were derived assuming electron densities of 1200 and 4200 cm^{-3} respectively, the average density yielded

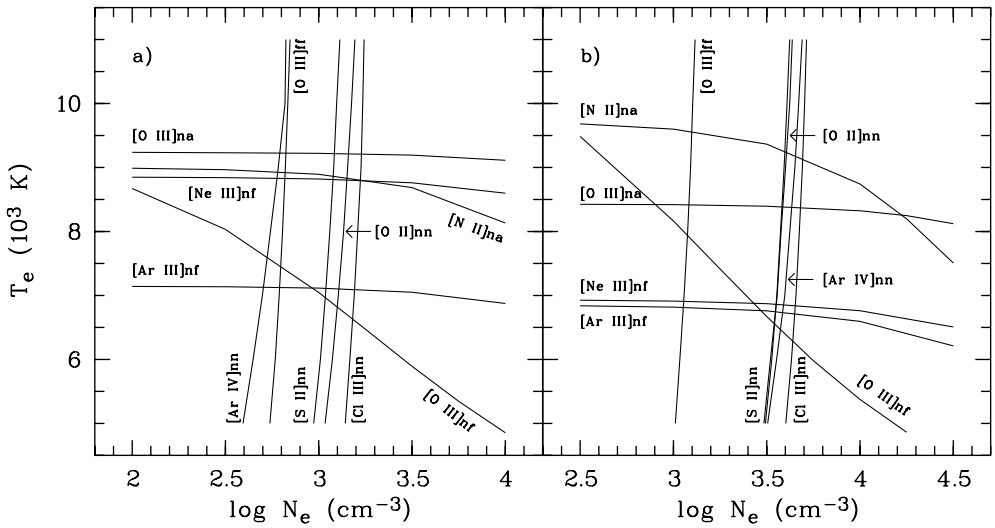

Figure 4. Plasma diagnostic diagrams for (a) M 1-42 and (b) M 2-36. The diagnostics are labelled by the ion and the lines involved – 'f' for (IR) fine-structure lines, 'n' for nebular forbidden lines, 'a' for auroral forbidden lines. Thus [O III]na represents [O III] nebular to auroral line ratio (λ4959 + λ5007)/λ4363, [O III]nf the nebular to far-IR fine-structure line ratio (λ4959 + λ5007)/(52 μm + 88 μm), and [O III]ff the far-IR fine-structure line ratio 88 μm/52 μm, and so on. The electron temperatures yielded by the [N II] nebular to auroral line ratio are probably overestimated because of contamination of the auroral line by recombination excitation.

Table 5. Extinction towards M 1-42 and M 2-36.

λ (Å)	$1/\lambda$ (μm^{-1})	M 1-42 $A(\lambda)$ (mag)	M 2-36 $A(\lambda)$ (mag)
6563	1.524	1.18	0.35
4861	2.057	1.77	0.72
4340	2.340	2.02	0.82
4101	2.438	2.12	0.91
3970	2.519		0.97
3835	2.608	2.27	0.97
3797	2.634	2.46	1.05
3770	2.652	2.41	1.06
3750	2.667	2.20	0.95
3203[a]	3.123	2.40	1.37
1640	6.097	5.70	

[a] Derived from the He II λ3203 line; not included in the fitting of the extinction curve.

Table 6. Plasma diagnostics.

Diagnostic	M 1-42	M 2-36
	T_e (K)	
[O III] (λ4959 + λ5007)/λ4363	9220	8380
[O III] (88μm + 52μm)/(λ4959 + λ5007)	6870[a]	6320[b]
[Ne III] 15.5μm/λ3868	8810	6850
[Ar III] 9.0μm/λ7135	7110	6730
[N II] (λ6548 + λ6584)/λ5754	8870[c]	9260[c]
[O II] (λ7320 + λ7330)/λ3727	16850[d]	14490[d]
BJ/H 11	3560	5900
	N_e (cm^{-3})	
[O III] 88μm/52μm	670	1210
[Ar IV] λ4740/λ4711	610	4370
[Cl III] λ5537/λ5517	1690	4830
[O II] λ3729/λ3726	1440	3880
[S II] λ6731/λ6716	1220	3840
Balmer decrement	$\lesssim 10^4$	$\lesssim 10^4$

[a] For $N_e = 1200\,\mathrm{cm}^{-3}$. $T_e = 7420$ K for $N_e = 670\,\mathrm{cm}^{-3}$ as given by the [O III] 88μm/52μm ratio.
[b] For $N_e = 4200\,\mathrm{cm}^{-3}$. $T_e = 7920$ K for $N_e = 1210\,\mathrm{cm}^{-3}$ as given by the [O III] 88μm/52μm ratio.
[c] Neglecting recombination excitation of the auroral λ5754 line.
[d] Neglecting recombination excitation of both the nebular and auroral lines.

by several (mainly) density-sensitive diagnostic ratios. With the relatively low densities prevailing in both nebulae, then for an implicitly assumed homogeneous nebula, the temperatures derived are insensitive to the exact value of electron density adopted, except for those deduced from the [O III] nebular to far-IR fine-structure line ratio (λ4959 + λ5007)/(52 μm + 88 μm), owing to the fairly low critical densities of the 52- and 88-μm fine-structure lines. Of the five forbidden line density-diagnostics listed in Table 6, the densities deduced from them are insensitive to electron temperature, and the values given there were calculated assuming a temperature derived from the [O III] nebular to auroral line ratio (λ4959 + λ5007)/λ4363. Diagnostic diagrams for the two nebulae, which show in the $\log N_e$–T_e plane the constraints placed by the various line ratios, are presented in Fig. 4.

The [Ne III] λ3342 auroral line and [Ar III] λ5192 were marginally detected from M 2-36. The weak λ3342 line fell in the wing of the much stronger nearby O III λ3340 line and was difficult to measure accurately. We noted in Section 2.1 that the [Ne III] λ3967 line in M 2-36 is affected by absorption by the interstellar Ca II H line. As a consequence, only the [Ne III] λ3868 line was used to calculate the [Ne III] nebular to IR fine-structure line diagnostic ratio. Similarly, although the [Ne III] 15.6-μm line was well detected by the *ISO*, the weaker 36-μm line was only marginally detected in both nebulae. The large uncertainties in the current measurements of the [Ne III] 36-μm line also make the 15.6 μm/36.0 μm ratio not useful for density-diagnostic purposes. This was unfortunate as the [Ne III] fine-structure lines have much higher critical densities than the [O III] 52- and 88-μm lines, and thus should yield an unbiased (see below)

temperature-independent density for the whole nebula. Similarly, although both the [S III] 18.7- and 33.5-μm fine-structure lines have been detected, the low S/N ratios make their ratio useless for the purpose of density determination.

The observed ratios of [Ne III] λ3868/λ3342 and [Ar III] λ7135/λ5192 from M 2-36 yield electron temperatures of 10 700 and 8530 K, respectively. The associated uncertainties are however likely to be large. Better observations with a higher spectral resolution are needed for the weak λ3342 and λ5192 lines to provide more reliable temperature determinations. Note that the SWS flux of the [Ne III] 15.6-μm line of M 2-36 was derived from the upward-scan only (Section 2.2) which was partially affected by cosmic rays. So the temperature derived from its ratio to the optical λ3868 nebular line should be treated with some caution.

M 1-42 and M 2-36 have an excitation class similar to that of NGC 6153, with most of C, N and O in their doubly ionized stages. As in the case of NGC 6153, the C, N and O and Ne abundances derived for them from ORLs are significantly higher than those derived from CELs (cf. Section 4). In Paper I we showed that in addition to electron collisional excitation, recombination can also play an important role in exciting the [N II] λ5754 auroral line as well as the [O II] λλ3726, 3729 nebular lines and λλ7320, 7330 auroral lines. While this does not affect the electron density deduced from the [O II] doublet ratio λ3729/λ3726, it can lead to apparently high electron temperatures derived from the [N II] nebular to auroral line ratio, (λ6548 + λ6584)/λ5754, and from the [O II] nebular to auroral line ratio, (λ3726 + λ3729)/(λ7320 + λ7330). In the case of M 1-42 and M 2-36, the [O II] nebular to auroral line ratio yields an electron temperature of 16 800 K (for $N_e = 1200\,cm^{-3}$) and 14 500 K (for $N_e = 4200\,cm^{-3}$), respectively, significantly higher than the corresponding values derived from the [O III] nebular to auroral line ratio (λ4959 + λ5007)/λ4363. For lower electron densities, the resultant temperatures would be even higher. The electron temperatures derived from the [N II] ratios show better agreement with the [O III] temperatures. For M 1-42, the [N II] temperature is actually slightly lower (but probably consistent within the errors) than the [O III] temperature. For M 2-36, the [N II] temperature is about 1000 K higher.

For a uniform nebula of low electron density such that collisional de-excitation can be neglected, the contributions to the [N II] auroral line and the [O II] nebular and auroral lines by recombination excitation can be calculated using equations (1) and (2) given in Paper I. Because of the relatively low critical densities of these lines, in particular of the [O II] nebular lines, their emissivities depend not only on electron temperature and the ionic abundances, but also on electron density. To estimate their intensities, it is thus necessary to solve the level populations for a multi-level atomic model, incorporating both collisional and recombination excitation. The interpretation of these lines can be further complicated if the nebula contains high-density condensations, or has temperature and/or chemical inhomogeneities. A detailed discussion of the formation mechanisms of these lines was presented in Sections 3.3 and 5.5 of Paper I. Given the uncertainties in the electron temperatures yielded by the [N II] and [O II] lines, they will be ignored in the abundance analysis detailed in the next section.

Liu (1997; see also Liu et al. 2001) compared the electron densities deduced from the [O III] 88 μm/52 μm ratio with those derived from the optical [Ar IV] and [Cl III] doublet ratios for a large sample of PN, and found that the density deduced from the 88 μm/52 μm ratio is systematically lower than those yielded by the latter two density-diagnostics for the same object, suggesting the presence of density inhomogeneities within the nebula. The same observational pattern is apparent here. For both objects, the four optical density diagnostics, i.e. the [Ar IV], [Cl III], [O II] and [S II] doublet ratios, yield very similar densities, which are significantly higher, by respectively a factor of 2 and 3.5 for M 1-42 and M 2-36, than those given by the far-IR [O III] fine-structure line 88 μm/52 μm ratio. The only exception is the [Ar IV] doublet ratio in M 1-42, which yields a density similar to that given by the 88 μm/52 μm ratio. This is likely caused by the uncertainties in the measurement of the [Ar IV] ratio. The [Ar IV] λλ4711, 4740 doublet lines have critical densities of 1.4×10^4 and $1.3 \times 10^5\,cm^{-3}$, respectively (for $T_e = 10^4$ K), the highest amongst all the density-diagnostic lines listed in Table 6. At the very low density prevailing in M 1-42, the λ4740/λ4711 ratio is no longer sensitive to density and a small error in the measurement of the λ4740/λ4711 ratio leads to a large uncertainty in the derived density. In fact, for M 1-42 the observed λ4740/λ4711 ratio, 0.761, is within 8 per cent of its low-density limit of 0.703. The formal errors as estimated from the Gaussian line profile fitting of the λ4711 and λ4740 lines are 8.0 and 2.6 per cent, respectively, which translate into an error of 8.4 per cent in the resultant λ4740/λ4711 ratio, leading to a density ranging from 0 up to $1300\,cm^{-3}$. The upper limit is thus consistent with densities deduced from other density diagnostics, such as the [Cl III], [O II] and [S II] doublet ratios.

Fig. 4 and Table 6 show that for both nebulae, the electron temperatures deduced from the ratios of the IR fine-structure lines to the optical nebular lines are systematically lower than those deduced from the [O III] nebular to auroral line ratio. Owing to the relatively low critical densities of the [O III] far-IR fine-structure lines, the electron temperatures derived from their ratio to the corresponding nebular lines are sensitive to the adopted electronic density (Fig. 4). However, even for the very low electron density given by the [O III] 88 μm/52 μm ratio, the resultant temperatures are still lower, by ∼1800 and 500 K, for M 1-42 and M 2-36 respectively, than the corresponding values yielded by the [O III] (λ4959 + λ5007)/λ4363 ratio. More importantly, the observed ratios of the [Ne III] and [Ar III] infrared fine-structure to optical nebular lines also yield lower temperatures. Because of the much higher critical densities of the [Ne III] and [Ar III] IR fine-structure lines, the electron temperatures derived from their ratios to the corresponding optical nebular lines are essentially density-independent, unless the density is significantly higher than $\gtrsim 10^5\,cm^{-3}$ (Fig. 4). Thus, provided that both Ne^{2+} and Ar^{2+} arise from similar ionization regions as O^{2+}, which is likely the case given the similar ionization potentials of the O^+, Ne^+ and Ar^+ ions, the discrepancies between the electron temperatures deduced from the [O III] optical nebular to auroral line ratio and those deduced from the ratios of optical nebular lines to IR fine-structure lines cannot be entirely caused by density inhomogeneities (unless there are clumps with $N_e \gtrsim 10^6\,cm^{-3}$, which seems however unlikely given the low densities implied yielded by the observed Balmer decrement; see below). Instead, the result points to the presence of significant temperature fluctuations (Peimbert 1967) in these two nebulae.

The electron temperatures deduced from the ratio of the nebular continuum Balmer discontinuity to H 11 are included in Table 6 and are 3560 and 5900 K for M 1-42 and M 2-36, respectively. The emissivities for the H I, He I and He II continua published by Brown & Mathews (1970) cover a temperature range from 4000 to 20 000 K. For M 1-42, the observed Balmer jump to H 11 ratio,

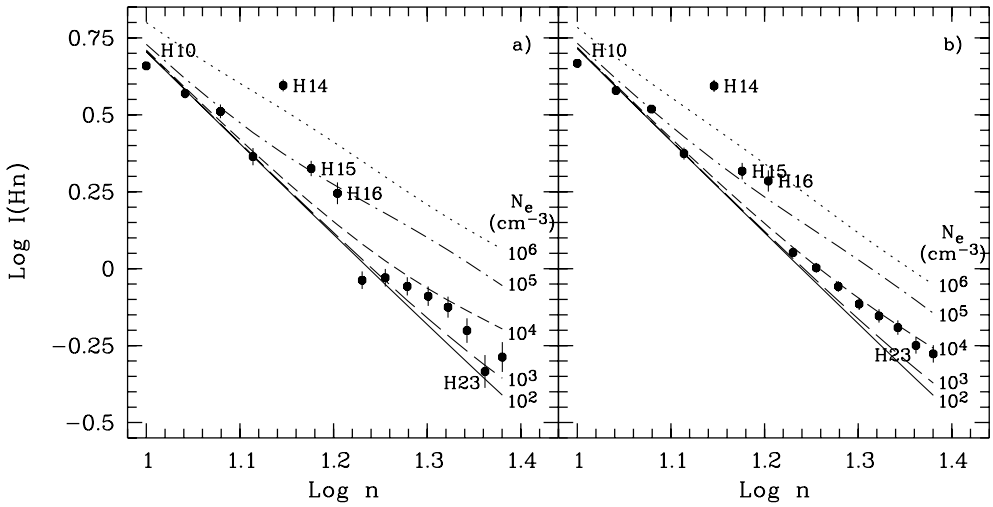

Figure 5. Observed intensities (in units where H$\beta = 100$) of high-order Balmer lines ($n \rightarrow 2$, $n = 10$–24) as a function of principle quantum number n, for (a) M 1-42 and (b) M 2-36. H 14 at 3721.94 Å is blended with the [S III] λ3721.63 line. H 15 at 3711.97 Å and H 16 at 3703.86 Å may also be contaminated by some weak unknown lines. The various curves show respectively, the predicted Balmer decrements for electron densities from $N_e = 10^2$ to $10^6\,cm^{-3}$, assuming an electron temperature of 3560 K for M 1-42 and 5900 K for M 2-36, as deduced from the ratio of the nebular continuum Balmer discontinuity to H 11.

BJ/H 11 $\equiv [I_c(\lambda3643) - I_c(\lambda3681)]/I$(H 11), is so large that, for the given He^+/H^+ and He^{2+}/H^+ ionic abundances, it is even higher than the value predicted for an electron temperature of 4000 K. There is however a simple relation between the Balmer jump and the plasma electron temperature,

$$T_e = 368 \times (1 + 0.259y^+ + 3.409y^{++}) \left(\frac{\text{BJ}}{\text{H 11}}\right)^{-3/2} \text{K}, \qquad (3)$$

where BJ/H 11 is in units of $Å^{-1}$ and $y^+ \equiv He^+/H^+$ and $y^{++} \equiv He^{++}/H^+$ are respectively, the ionic abundances of singly and doubly ionized He. This equation has been used to calculate the Balmer jump temperatures, T_e(BJ/H 11), of M 1-42 and M 2-36 tabulated in Table 6, using the He^+/H^+ and He^{++}/H^+ abundance ratios derived in Section 8. Since the He^+/H^+ and He^{++}/H^+ ratios deduced from the He I and He II recombination lines also have a weak dependence on electron temperature, the process was iterated such that self-consistent values for the He^+/H^+ and He^{++}/H^+ abundance ratios and T_e(BJ/H 11) were reached.

The Balmer jump temperature of 3560 K for M 1-42 is probably the lowest Balmer jump temperature that has ever been derived for a PN or H II region. The very low Balmer jump temperatures deduced for M 1-42 and M 2-36 are consistent with the systematically lower temperatures yielded by ratios of optical nebular lines to IR fine-structure (forbidden) lines compared to those deduced from optical [O III] nebular to auroral line ratios – both results point to the presence of large temperature fluctuations in the nebulae. For M 2-36, the observed [O III] nebular to auroral ratio temperature and the Balmer jump temperature yield a mean temperature $T_0 = 6470$ K and a temperature fluctuation parameter $t^2 = 0.053$ (Peimbert 1971). The latter corresponds to a temperature fluctuation amplitude of 23 per cent. For M 1-42, the [O III] temperature is nearly a factor of 3 higher than the Balmer jump temperature and we find $T_0 = 4470$ K and $t^2 = 0.122$, or a fluctuation amplitude of 35 per cent.

Fig. 5 plots the observed high-order Balmer decrement ($n \rightarrow 2$, $n = 10$–24) as a function of the principle quantum number n of the upper level. Overplotted are predicted Balmer decrements for different electron densities (Storey & Hummer 1995). Fig. 5 shows that for both nebulae, the bulk of hydrogen emission arises from regions with $N_e \lesssim 10^4\,cm^{-3}$, consistent with the electron densities derived from various forbidden line density diagnostics, i.e. there is no evidence of a substantial amount of *ionized* high-density ($N_e \gtrsim 10^6\,cm^{-3}$) material in these nebulae unless such material is also hydrogen deficient (Paper I). Note that the Balmer decrement becomes sensitive to the electron density only for $n \gtrsim 10$. Given the small wavelength span of the Balmer lines from $n = 10$ up to 24, the highest Balmer line we can measure in our spectra, the Balmer decrement density implied by the data plotted in Fig. 5 should be fairly insensitive to the uncertainties in the reddening corrections and should be unaffected by the fact that we have used the lower order Balmer lines, from Hα to H 12 at 3750 Å to derive the reddening law towards M 1-42 and M 2-36.

The C II resonance line $2s^2 2p\,^2P^o$–$2s\,^2p^2\,^2D$ λ1335 has been clearly detected by the *IUE* in M 2-36 (Fig. 2). While the C II $2s^2 3d\,^2D$–$2s^2 4f\,^2F^o$ λ4267 line in the optical is mainly excited by radiative recombination, λ1335 emission is dominated by dielectronic recombination, formed by the allowed radiative decay from the autoionizing states $2s2pnd\,^2P^o$ and $^2F^o$. (We can ignore collisional excitation of this resonance doublet at the temperature inferred for M 2-36.) Thus the intensity of the λ1335 line has a strong dependence on T_e, and as a consequence, the observed intensity ratio $\lambda1335/\lambda4267$ can be used to derive the electron temperature. The obvious advantage of the $\lambda1335/\lambda4267$ ratio as a temperature diagnostic is that both lines are formed by recombination, thus the result should provide an interesting comparison to that given by the Balmer discontinuity, which is also formed by recombination. The $\lambda1335/\lambda4267$ temperature-diagnostic ratio has been used previously by Ferland et al. (1984) to determine the electron temperature in the ejecta of the classical nova DQ Her. They obtained a value of 700 K, in corroboration of Williams et al. (1978) who adopted an electron temperature of 500 K in their abundance determinations for DQ Her. The application of this diagnostic to PN is however complicated in practice as λ1335 emission may be subject to a number of destruction mechanisms, such as self-absorption, and absorption by intervening interstellar diffuse clouds and dust particles (both

Table 7. Ionic abundances from CELs[a].

X^{i+}/H^+	Lines	M 1-42	M 2-36
C^{2+}/H^+	C III] λ1908	8.67(−5)	4.46(−4)
N^+/H^+	[N II] λλ6548,6584	5.86(−5)	4.26(−5)
	[N II] 122 μm	1.03(−4)[b]	
	[N III] 57 μm	3.48(−4)[c]	1.98(−4)[c]
O^+/H^+	[O II] λλ3726,3729	3.88(−5)[d]	8.59(−5)[d]
O^{2+}/H^+	[O III] λλ4959,5007	2.49(−4)	5.48(−4)
	[O III] 52, 88 μm	5.10(−4)[e]	6.70(−4)[e]
O^{3+}/H^+	[O III] 25.9 μm	4.18(−6)[f]	
Ne^{2+}/H^+	[Ne III] λλ3868	9.62(−5)	1.67(−4)
	[Ne III] 15.5 μm	1.14(−4)[g]	4.27(−4)[g]
S^+/H^+	[S II] λλ6716,6731	1.28(−6)[h]	1.51(−6)[h]
S^{2+}/H^+	[S III] λλ6312	4.70(−6)	7.49(−6)
	[S III] 18.7, 33.5 μm	1.02(−5)[i]	2.66(−5)[i]
S^{3+}/H^+	[S IV] 10.5 μm	2.22(−6)[j]	8.32(−6)[j]
Cl^{2+}/H^+	[Cl III] λλ5517,5537	1.13(−7)	1.51(−7)
Ar^{2+}/H^+	[Ar III] λ7135	1.86(−6)	2.45(−6)
	[Ar III] 9.0 μm	3.36(−6)[k]	4.20(−6)[k]
Ar^{3+}/H^+	[Ar IV] λλ4711,4740	3.68(−7)	5.13(−7)

[a] Assuming $T_e = 9220$ K, $N_e = 1200\,cm^{-3}$ for M 1-42 and $T_e = 8380$ K, $N_e = 4200\,cm^{-3}$ for M 2-36 unless otherwise specified. The numbers in parentheses are powers of 10.
[b] For $N_e = 670\,cm^{-3}$ as deduced from the far-IR low critical-density diagnostic ratio [O III] 88μm/52μm ratio. For $N_e = 1200\,cm^{-3}$, $N^+/H^+ = 1.71(-4)$.
[c] Assuming $N_e = 670$ and $1210\,cm^{-3}$ for M 1-42 and M 2-36, respectively. For M 1-42, $N^{2+}/H^+ = 5.04(-4)$ for $N_e = 1200\,cm^{-3}$, whereas for M 2-36, $N^{2+}/H^+ = 5.47(-4)$ for $N_e = 4200\,cm^{-3}$.
[d] Upper limit as a result of possible recombination excitation of the [O II] λλ3726, 3729 doublet (Liu et al. 2000).
[e] Assuming $N_e = 670$ and $1210\,cm^{-3}$ for M 1-42 and M2-36, respectively. $O^{2+}/H^+ = 6.77(-4)$ for M 1-42 if $N_e = 1200\,cm^{-3}$, whereas $O^{2+}/H^+ = 1.53(-3)$ for M 2-36 if $N_e = 4200\,cm^{-3}$.
[f] For $N_e = 670\,cm^{-3}$. $O^{3+}/H^+ = 4.78(-6)$ for $N_e = 1200\,cm^{-3}$.
[g] For M 1-42, $Ne^{2+}/H^+ = 1.13(-4)$ if $N_e = 670\,cm^{-3}$, whereas for M 2-36, $Ne^{2+}/H^+ = 4.13(-4)$ if $N_e = 1210\,cm^{-3}$.
[h] For M 1-42, $S^+/H^+ = 1.18(-6)$ for $N_e = 670\,cm^{-3}$ and for M 2-36, $S^+/H^+ = 1.06(-6)$ for $N_e = 1210\,cm^{-3}$.
[i] For M 1-42, $S^{2+}/H^+ = 8.90(-6)$ if $N_e = 670\,cm^{-3}$, whereas for M 2-36, $S^{2+}/H^+ = 1.68(-5)$ if $N_e = 1210\,cm^{-3}$.
[j] For M 1-42, $S^{3+}/H^+ = 2.14(-6)$ for $N_e = 670\,cm^{-3}$, whereas for M 2-36, $S^{3+}/H^+ = 6.98(-6)$ for $N_e = 1210\,cm^{-3}$.
[k] For M 1-42, $Ar^{2+}/H^+ = 3.35(-6)$ for $N_e = 670\,cm^{-3}$ and for M 2-36, $Ar^{2+}/H^+ = 4.08(-6)$ for $N_e = 1210\,cm^{-3}$.

internal and interstellar). All these processes will suppress the observed λ1335/λ4267 ratio and consequently the apparent electron temperature derived from it. In a typical PN, C II resonance transitions are almost certain to be optically thick, as indicated by the fact that all case-sensitive ORLs from singly ionized CNO and Ne ions follow Case B recombination, rather than Case A (Liu et al. 1995; 2000). For M 2-36, our observations yield a λ1335/λ4267 ratio of 16.4, more than a factor 2 lower than the value of 43 predicted for the Balmer jump temperature of 5900 K for M 2-36. Here we have used the C II effective recombination coefficients calculated recently by Davey, Storey & Kisielius (2000). In fact, the observed ratio would have yielded a T_e of only 2000 K, a value possibly too low to be realistic and possibly indicating that the λ1335 line has been suppressed by absorption effects. High spectral resolution observation of the λ1335 line is however needed to clarify the situation.

Table 8. He abundances.

He^{i+}/H^+	Line	M 1-42	M 2-36
He^+/H^+	He I λ4471	0.132	0.127
He^+/H^+	He I λ5876	0.141	0.133
He^+/H^+	He I λ6678	0.138	0.138
He^+/H^+	Mean	0.139	0.133
He^{2+}/H^+	He II λ4686	0.009	0.003
He/H		0.148	0.135

5 ABUNDANCE ANALYSIS

5.1 Ionic abundances from CELs

The ionic abundances deduced from detected UV, optical and infrared CELs are presented in Table 7. The electron temperature deduced from the [O III] nebular to auroral line ratio has been adopted for all ionic species for both nebulae. We have shown in the last section that temperature diagnostics based on the ratios of optical forbidden lines to IR fine-structure lines tend to yield lower temperatures, as does the Balmer jump to H 11 ratio produced by recombination. Since the main purpose of the current paper is to compare heavy element abundances derived from the traditional CEL method to those deduced from ORLs, and since in standard CEL abundance analyses, the [O III] nebular to auroral line ratio serves as the standard and often the sole temperature diagnostic, temperatures yielded by other diagnostics are not used.

For the electron densities, we have adopted the mean values deduced from the various optical diagnostics, i.e. $N_e = 1200$ and $4200\,cm^{-3}$ for M 1-42 and M 2-36, respectively. However, for a few far-IR fine-structure lines with relatively low critical densities, [N II] 122 μm, [N III] 57 μm and [O III] 52 and 88 μm, the density deduced from the [O III] 88 μm/52 μm ratio was used. For the majority of the other abundance diagnostic lines listed in Table 7, the differences between the deduced ionic abundances based on the two assumed densities for each nebula are negligible, given their higher critical densities. One exception is the S^+/H^+ abundance ratio in M 2-36 derived from the [S II] optical doublet λλ6716, 6731. For ionic abundances based on the IR fine-structure lines, both values deduced for the two adopted densities are provided in Table 7, with the adopted one listed in the main part of the table and the other value in the footnotes for easy comparison.

The [Ne III] 36-μm line was only marginally detected, so only the 15.6-μm line was used in calculating the Ne^{2+}/H^+ fine-structure line abundance. For [S III], both the 18.7- and 33.5-μm lines have comparable (relatively low) S/N and their fluxes are co-added before calculating a combined S^{2+}/H^+ abundance ratio.

The UV intercombination line O III] λ1664 detected in the *IUE* spectrum of M 1-42 yields $O^{2+}/H^+ = 3.22 \times 10^{-3}$, much higher than those deduced from [O III] optical and far-IR lines. The feature could well be spurious and caused by, for example, the detector defects discussed by Crenshaw, Bruegman & Norman (1990). We will thus ignore this result. For M 2-36, the N III] λ1751 line, marginally detected by the *IUE*, yields $N^{2+}/H^+ = 9.31 \times 10^{-4}$, which is within a factor of 2 of that deduced from the 57-μm line. Since the line was only marginally detected and the aforementioned *IUE* detector defects also affect the λ1751 wavelength region, this result will be ignored as well.

5.2 Ionic abundances from ORLs

5.2.1 He^+/H^+ and He^{++}/H^+

Ionic abundances deduced from ORLs are presented in Table 8 for He^+/He, He^{2+}/H^+ and in Tables 10–13 and 15–16 for C^{2+}/H^+, N^{2+}/H^+, O^{2+}/H^+, Ne^{2+}/H^+, plus C^{3+}/H^+ and N^{3+}/H^+. ORL abundances have only a weak dependence on the adopted electron temperature, $X^{i+}/H^+ \propto T_e^{\alpha}$, where $|\alpha| \ll 1$, and are essentially independent of the electron density under the low-density conditions ($\ll 10^6\,cm^{-3}$) prevailing in most nebulae. In our previous analysis of NGC 6153 (Liu et al. 2000), the electron temperature deduced from the [O III] nebular to auroral line ratio was used to calculate ionic abundances from both ORLs and from CELs. Given the more than a factor of 2 difference between the Balmer jump and the [O III] forbidden line temperatures in M 1-42, we decided to use the Balmer jump temperature, 3560 and 5900 K, for M 1-42 and M 2-36, respectively, to calculate the ORL abundances, in an effort to maintain a self-consistent ORL analysis. For the electron density, representative values of 1200 and $4200\,cm^{-3}$ have been assumed for M 1-42 and M 2-36, respectively, i.e. the same as those adopted for the CEL abundance analysis.

The ORL ionic abundances presented here were derived using the same atomic data as described by Liu et al. (2000), except for He^+/H^+ (Table 8). The effective recombination coefficients of He I lines given by Brocklehurst (1972) were calculated for a temperature range from 5000 to 20 000 K. To allow for the very low Balmer jump temperature in M 1-42, we have used the more recent calculations of Smits (1996) who gives effective recombination coefficients for a number of selected He I lines for temperatures down to as low as 312.5 K. Over the temperature range common to both calculations, the effective recombination coefficients given by Brocklehurst (1972) and Smits (1996) for the three He I lines used for abundance determinations differ by just a few per cent.

The ionic and total He/H abundances of M 1-42 and M 2-36 are given in Table 8. Given the low electron temperatures and densities in both nebulae, collisional excitation of the three He I abundance diagnostic lines is negligible and the He^+/H^+ abundances yielded by them agree with each other very well. The He/H abundance of M 2-36 is nearly identical to that of NGC 6153 (0.134–0.137; Paper I) and is moderately enhanced relative to the nearly solar value of 0.109 for NGC 7009 (Liu et al. 1995). The He enhancement in M 1-42 is higher, with a He/H ratio of 0.148. Such high He/H abundances are only found in a few extreme Type I bipolar PN, such as NGC 6302 and 6537 (Peimbert & Torres-Peimbert 1983; Kingsburgh & Barlow 1994).

In our previous analysis of NGC 6153 (Paper I), we noticed that while the observed intensities of the He I $2p\,^3P^o$–nd ^3D and $2p\,^1P^o$–nd ^1D series, relative to the λ4471 $2p\,^3P^o$–4d ^3D line, agreed well with those predicted by recombination theory, the intensities of the $2s\,^1S$–$np\,^1P^o$ and $2p\,^1P^o$–$ns\,^1S$ series were systematically lower than the predictions by a factor of 2–3 and 40 per cent respectively. The weakness of the $2s\,^1S$–$np\,^1P^o$ series is clearly caused by self-absorption from the metastable $2s\,^1S$ state. However such self-absorption should at the same time lead to the enhancement of the $2p\,^1P^o$–$ns\,^1S$ series, just the opposite of what is observed. In Table 9, the intensities of the He I lines observed in the

Table 9. Intensities of the He I lines, normalized such that I_r(He I λ4471) = 1.00. Collisional excitation, at the very low electron density and Balmer jump temperature observed for both nebulae, is negligible and is therefore neglected. The results are compared to the theoretical values deduced from Brocklehurst (1972) and Smits (1996) for $T_e = 5000$ K and $N_e = 10^4\,cm^{-3}$. Case A has been assumed for the triplets and Case B for the singlets.

λ_0	n	I_{obs} M 1-42	I_{obs} M 2-36	I_{pred} B72	I_{pred} S96
		$2s\,^1S$ – $np\,^1P^o$ series			
3447.59	6		.029	.055	
3613.64	5	.064	.053	.096	
		$2p\,^1P^o$ – $ns\,^1S$ series			
4437.55	5	.007	.010	.012	
5047.74	4			.030	
7281.35	3	.114	.095	.108	.113
		$2p\,^1P^o$ – $nd\,^1D$ series			
3805.74	11	.005	.006	.010	
3926.54	8	.016	.023	.027	
4009.26	7	.049	.036	.041	
4143.76	6	.066	.070	.069	
4387.93	5	.108	.103	.124	.120
4921.93	4	.261	.276	.275	.269
6678.16	3	.935	.894	.866	.847
		$2s\,^3S$ – $np\,^3P^o$ series			
3187.74	4	.807	.524	.745	.748
3888.65	3	1.70	1.38	1.90	1.86
		$2p\,^3P^o$ – $ns\,^3S$ series			
4120.84	5	.019	.028	.026	
4713.17	4	.088	.109	.065	.075
7065.25	3	.511	.867	.245	.356
		$2p\,^3P^o$ – $nd\,^3D$ series			
3465.94	17		.015	.011	
3471.83	16			.013	
3478.97	15	.049	.017	.015	
3487.73	14	.068	.012	.019	
3498.66	13	.033	.024	.023	
3512.52	12	.028	.031	.030	
3530.50	11	.054	.036	.038	
3554.42	10	.060	.044	.051	
3587.28	9	.055	.057	.071	
3634.25	8	.083	.088	.101	
3705.02	7	.101[a]	.070[a]	.154	
3819.62	6	.237	.224	.251	
4026.21	5	.490	.472	.449	.451
4471.50	4	1.00	1.00	1.00	1.00
5875.66	3	3.27	3.01	3.01	2.95

[a] Blended with λ3703.86 H 16.

Table 10. C^{2+}/H^+ abundances from ORLs.

λ_0 (A)	Mult	M1-42 I_{obs}	M1-42 $\frac{C^{2+}}{H^+}$ (10^{-3})	M2-36 I_{obs}	M2-36 $\frac{C^{2+}}{H^+}$ (10^{-3})
7231.3198	V3	.558	1.26	.433	1.02
7236.4199	V3	.919	1.03	.841	.99
V 3 $3p\,^2P^o$–$3d\,^2D$		**1.48**	**1.11**	**1.27**	**1.00**
3918.9800	V4	.036	3.12	.026	1.76
3920.6899	V4	.053	2.30	.047	1.59
V 4 $3p\,^2P^o$–$4s\,^2S$		**.089**	**2.57**	**.073**	**1.64**
V 6 $3d\,^2D$–$4f\,^2F^o$ λ4267		**2.55**	**1.98**	**2.47**	**2.14**

Table 11. N^{2+}/H^+ abundances from ORLs. λ4613.68 (V 92b) lines, using O II $I(\lambda4613.14 + \lambda4613.68)/I(\lambda4602.13) = 0.453$.

λ_0 (Å)	Mult	M1-42 I_{obs}	M1-42 $\frac{N^{2+}}{H^+}$ (10^{-3})	M2-36 I_{obs}	M2-36 $\frac{N^{2+}}{H^+}$ (10^{-3})
5666.63	V3	.673	5.67	.188	1.52
5676.02[k]	V3	.319	6.06	.078	1.42
5679.56	V3	1.27	5.77	.388	1.69
5686.21	V3	.205[k]	5.20	.075	1.83
5710.77	V3	.197	7.53	.090	3.30
V 3 $3s\,^3P^o$ – $3p\,^3D$		**2.70**	**5.87**	**.842**	**1.76**
4601.48	V5	.147	3.94	.034	.880
4607.16	V5	.107	3.59	.052	1.69
4621.39[a]	V5	.169	5.31	.054	1.33
4630.54	V5	.435	3.91	.140	1.22
4643.08[b,k]	V5	.199	5.38	.096	2.51
4613.87[c,k]	V5	.143	2.42	.066	1.00
V 5 $3s\,^3P^o$– $3p\,^3P$		**1.09**	**4.07**	**.343**	**1.24**
V 8 $3s\,^1P^o$ –$3p\,^1P$ λ6482				**.048**	**2.86**
V12 $3s\,^1P^o$ –$3p\,^1D$ λ3995		**.221**	**4.12**	**.043**	**0.70**
4788.13	V20	.131	3.31	.030	0.78
4803.29	V20	.318	4.50	.098	1.44
V 20 $3p\,^3D$ – $3d\,^3D^o$		**.695**	**4.08**	**.198**	**1.20**
5931.78[d]	V28	.231	3.56	.064	1.07
5940.24	V28	.063	3.23	.019	1.01
5941.65	V28	.353	3.23	.109	1.03
V 28 $3p\,^3P$ – $3d\,^3D^o$		**.793**	**3.38**	**.236**	**1.04**
		3d – 4f transitions			
4035.08[e]	V39a	.295	2.38	.125	1.10
4043.53	V39a	.261	1.73	.091	.690
4041.31[f]	V39b	.680	3.36	.225	1.24
4176.16	V43a	.183	1.97	.058	.720
4236.91	V48a	.169	3.02	.061	1.25
4241.24	V48a	.051	4.93	.017	1.88
4241.77	V48a	.685	5.72	.199	1.90
4179.67[g]	V48a	.071	4.63	.023[k]	1.97
4237.05[h]	V48b	.250	1.80	.090	0.74
4432.73[i]	V55a	.366	4.26	.116	1.54
4442.02	V55a	.087	2.69	.026	0.92
4552.53	V58a	.155	4.92	.068	2.41
4530.41[j]	V58b	.298	2.24	.117	.990
4678.14	V61b	.077	.92	.038	.520
Sum		**3.38**	**2.86**	**1.13**	**1.11**

[a] Corrected for the contributions from O II (V 92c) λ4621.27 and λ4622.14 [0.011 and 0.013 for M1-42 and M2-36, respectively, as estimated from $I(\lambda4510.20)$].
[b] Affected by nearby strong N III and O II emission.
[c] Corrected (45 and 65 per cent respectively for M1-42 and M2-36) for the contributions from the O II 3d–4f $^2D_{5/2}$–F[3]$_{5/2}$ λ4613.14 and $^2D_{5/2}$–F[3]$_{7/2}$.
[d] Corrected for a 5 per cent contribution from the He II λ5931.84 line using He II $I(\lambda5932)/I(\lambda4686) = 9.13 \times 10^{-4}$.
[e] Corrected for a 7 and 11 per cent contribution from O II 3d $^4F_{5/2}$–4f F[3]$_{5/2}$ λ4035.06 (V 50b), for M1-42 and M2-36 respectively, using O II $I(\lambda4035.06)/I(\lambda4089.29) = 0.027$.
[f] Corrected for a 3 and 5 per cent contribution from the O II 3d–4f $^4F_{5/2}$–F[2]$_{5/2}$ λ4041.29 and $^4F_{5/2}$–F[2]$_{3/2}$ λ4041.95 (V 50c) lines, for M1-42 and M2-36 respectively, using O II $I(\lambda4041.29 + \lambda4041.95)/I(\lambda4089.29) = 0.024$.
[g] Includes an 11 per cent contribution from N II 3d $^3D_3$–4f 2[3]$_2$λ4178.86 (V 50a).
[h] Includes N II λ4236.91(V 48a).
[i] Includes λ4433.48(V 55b), λ4431.82(V 55a).
[j] Corrected for a 1 and 2 per cent contribution from N III λ4530.86, for M1-42 and M2-36 respectively, using N III $I(\lambda4530.86)/I(\lambda4514.86) = 0.042$.

spectra of M 1-42 and M 2-36 are compared to the predictions of recombination theory. Similar patterns in the relative intensities of the He I lines as seen in NGC 6153 are apparent here.

Under typical nebular conditions, it is generally assumed that the He I Lyman series $2s^2\,^1S$–$1snp\,^1P^o$ lines are optically thick and that the He I singlet transitions obey Case B recombination theory. Under this assumption, all the Lyman photons emitted by transitions from upper levels $n \geq 3$ of singlet He I will be re-absorbed and scattered by neutral He^0, and eventually converted to He I Ly α at 584 Å plus photons at longer wavelengths, in particular those of the series $2s\,^1S$–$np\,^1P^o$. Of the three singlet series tabulated in Table 9, the $2p\,^1P^o$–$nd\,^1D$ series is essentially unaffected by optical depth effects and the assumption of Case A or Case B recombination. On the other hand, the predicted intensities of the other two singlet series, $2s\,^1S$–$np\,^1P^o$ and $2p\,^2P^o$–$ns\,^1S$, are strongly affected. For Case A recombination, the predicted intensities of the $2s\,^1S$–$np\,^1P^o$ series, relative to λ4471, are more than an order or magnitude lower than those predicted for Case B. For the $2p\,^2P^o$–$ns\,^1S$ series, the predicted Case A intensities are approximately a factor of 2 lower than for Case B. However, having wavelengths $\lesssim 584$ Å, shorter than the H I Lyman limit at 912 Å, the He I Lyman photons are capable of ionizing neutral hydrogen atoms. He I Lyman photons can also be destroyed by dust absorption. Thus, if there is a significant amount of neutral hydrogen or dust grains co-existing with He^+, it is possible that many of the He I Lyman photons emitted by recombinations of the He^+ ions are destroyed by photoionization of H^0 or absorption by dust grains, rather than re-absorbed by He^0 and converted to photons at longer wavelengths, effectively causing a departure of the He I singlet recombination spectrum from pure Case B recombination towards Case A, even though the nebula is optically thick in the He I Lyman series. Detailed photoionization modelling is needed to test whether this hypothesis can explain quantitatively the observed intensities of the He I $2p\,^2P^o$–$ns\,^1S$ and $2s\,^1S$–$np\,^1P^o$ series. If confirmed, the observed intensities of the He I $2p\,^2P^o$–$ns\,^1S$ series could potentially provide a diagnostic to probe the nebular ionization structure and the radiation transfer of the He I diffuse ionizing radiation fields.

5.2.2 C^{2+}/H^+ abundances from ORLs

C^{2+}/H^+ derived from three C II multiplets, V 3, 4 and 6, are given in Table 10. The upper levels of multiplets V 3 and 4 can cascade down to the C II $2p\,^2P^o$ ground level and thus their emissivities depend strongly on the optical depths of the C II resonance lines. Here Case B recombination has been assumed for multiplets V 3 and 4. The C^{2+}/H^+ abundances thus derived from multiplet V 3, which is well observed in both nebulae, are about a factor of 2 smaller than those derived from multiplet V 6 at 4267 Å, which is essentially case insensitive, suggesting that there is some small departure from the Case B recombination. The doublet from multiplet V 4 was clearly seen in M 2-36 but was only marginally detected from M 1-42. For M 2-36, this multiplet also yields a slightly lower abundance than λ4267.

In NGC 6153, we detected several high-excitation C II ORLs, including two lines from the 4f–*n*g series which feeds the λ4267 line, λ6462 ($n = 6$) and λ5342 ($n = 7$), as well as 4p–5d λ6259

[k] Of a low S/N, or blended with other lines, and not included in calculating the average abundance and the total intensity of the multiplet.

Table 12. O^{2+}/H^+ abundances from 3–3 recombination lines.

λ_0 (Å)	Mult	M1-42 I_{obs}	M1-42 $\frac{O^{2+}}{H^+}$ (10^{-3})	M2-36 I_{obs}	M2-36 $\frac{O^{2+}}{H^+}$ (10^{-3})
4638.85 [a,f]	V1	.693	6.79	.520	5.10
4641.81 [a,f]	V1	1.15	4.45	.816	3.17
4649.13	V1	1.76	3.60	1.36	2.77
4650.84	V1	.534	5.24	.371	3.64
4661.63	V1	.620	4.76	.432	3.32
4673.73	V1	.132	6.54	.081	4.01
4676.23	V1	.437	3.99	.312	2.85
4696.35	V1	.067	5.53	.047	3.88
V 1 3s ^{4}P–3p ^{4}D°		**5.03**	**4.11**	**3.68**	**3.01**
4317.14	V2	.233	3.09	.191	2.55
4319.63	V2	.209	2.56	.136	1.68
4325.76	V2	.036[f]	2.39	.048	3.21
4345.56[b]	V2	.444	5.60	.295	3.77
4349.43	V2	.556	2.95	.390	2.08
4366.89	V2	.360	4.47	.260	3.25
V 2 3s ^{4}P–3p ^{4}P°		**1.92**	**3.55**	**1.37**	**2.55**
4414.90	V5	.225	5.37	.166	3.63
4416.97	V5	.188	8.08	.139	5.48
4452.37	V5	.042	9.08	.022	4.36
V 5 3s ^{2}P–3p ^{2}D°		**.442**	**6.34**	**.327**	**4.29**
4069.62,.89	V10	1.35	5.07	1.21	4.65
4072.16	V10	1.30	5.24	.963	3.97
4075.86	V10	1.36	3.79	1.11	3.16
4078.84	V10	.215	5.71	.147	3.98
4085.11	V10	.228	4.93	.162	3.57
4092.93	V10	.199	5.90	.140	4.23
V 10 3p ^{4}D°–3d ^{4}F		**4.66**	**4.70**	**3.75**	**3.85**
3907.46	V11			.034	3.31
V 11 3p ^{4}D°–3d ^{4}P				**.097**	**3.31**
3851.03	V12			.032[f]	3.84
3882.19,83.13[c]	V12	.240	6.10	.184	4.49
V 12 3p ^{4}D°–3d ^{4}D		**.495**	**6.10**	**.353**	**4.49**
4121.46	V19	.155	5.24	.115	4.01
4129.32	V19	.057	8.23	.028[r]	4.17
4132.80	V19	.233	4.03	.180	3.21
4153.30	V19	.412	4.99	.283	3.53
4156.53[e,f]	V19	.143	10.9	.142	11.1
4169.22[d]	V19	.146	4.29	.134	3.60
V 19 3p ^{4}P°–3d ^{4}P		**1.05**	**4.77**	**.749**	**3.52**
4110.79	V20	.120	4.72	.094	3.81
4119.21,20.28,.20.54	V20	.641	5.24	.472	3.98
V 20 3p ^{4}P°–3d ^{4}D		**1.19**	**5.12**	**.889**	**3.96**
4699.22	V25	.054	7.73	.042	6.20
4705.35	V25	.103	8.96	.024	2.15
V 25 3p ^{2}D°–3d ^{2}F		**.161**	**8.49**	**.068**	**3.68**
4890.86	V28	.044[f]	3.57	.042	3.52
4906.83	V28	.161	6.10	.093	3.64
4924.53	V28	.284	6.32	.213	4.89
V 28 3p ^{4}S°–3d ^{4}P		**.522**	**6.24**	**.348**	**4.29**
4941.07	V33			.029	12.3
4943.00	V33	.049	10.0	.040	8.60
V 33 3p ^{2}P°–3d ^{2}D		**.082**	**10.0**	**.076**	**9.84**

[a] Affected by nearby strong N III lines.
[b] Includes a 5 per cent contribution from O II $3d\,^4D_{7/2}$ – $4f\,G[3]_{7/2}$ λ4345.55 (V 65c).
[c] Corrected for the contribution from O II λ3882.45 (V 11), estimated to be $I_{obs} = 0.013$ and 0.022 for M1-42 and M2-36, respectively, using λ3907.46 of the same multiplet.

and 4d–6f λ6151 (Paper I). Their observed intensities relative to λ4267 are in good agreement with the predictions of recombination theory. The λ6462, λ5342 and λ6151 lines have also been detected in M 2-36, with intensities relative to λ4267 that are within 40 per cent of the predicted values. The λ4802 (4f–8g) and λ4491 (4f–9g) transitions are marginally detected, but their intensities are uncertain because of the low S/N and blending with other lines.

For both nebulae, we will adopt the C^{2+}/H^+ abundance ratio derived from the λ4267 line alone.

5.2.3 N^{2+}/H^+ abundances from ORLs

N^{2+}/H^+ ratios derived from N II ORLs are presented in Table 11. Lines from 3s–3p, 3p–3d and 3d–4f configurations, both singlet and triplet, have been detected. Unlike other doubly ionized species, e.g. C^{2+}, O^{2+} and Ne^{2+}, for which the ionic abundances relative to H^+ derived from the lower excitation 3s–3p transitions tend to be smaller than those derived from 3p–3d and 3d–4f transitions with higher excitation energies, in the case of N^{2+}/H^+ the abundances deduced for M 1-42 and M 2-36 from the N II 3s–3p multiplets (V 3 and 5) are significantly higher than those derived from the 3d–4f transitions. The emissivity of multiplet V 5 is very sensitive to the optical depths of the N II resonance lines $2p\,^3P^o$–$nl\,^3S$, ^3D. For Case A recombination, the N^{2+}/H^+ abundances derived from multiplet V 5 would be a factor of 5 higher than those listed in Table 11, calculated assuming Case B recombination. However, multiplet V 3 is much less sensitive to optical depth effects – the Case A effective recombination coefficient of multiplet V 3 is only 20 per cent lower than the Case B value. The discrepancy between N^{2+}/H^+ ratios derived from 3s–3p multiplets and those derived from 3d–4f transitions is most significant for M 1-42, where multiplet V 3 gives an N^{2+}/H^+ abundance ratio which is a factor of 2 higher than the average value yielded by the 3d–4f transitions. V 3 is one of the strongest N II multiplets observable in the optical and is well measured for both M 1-42 and M 2-36. Observational uncertainties as the cause of the discrepancy can be ruled out. Multiplet V 3 also yields a slightly higher N^{2+}/H^+ abundance than the 3d–4f transitions in NGC 6153, but by only 15 and 30 per cent for the two sets of spectra we analysed (Paper I), which is probably insignificant given the possible uncertainties in the observations and atomic data. Multiplet V 3 was not measured by Liu et al. (1995) in NGC 7009 and the ORL N^{2+}/H^+ abundance determined by them for NGC 7009 was based on the two strongest transitions from the 3d–4f configuration, λλ4041,4043. Echelle spectroscopic observations from 3650 to 10 050 Å for two regions in the bright shell of NGC 7009 were presented by Hyung & Aller (1995a,b). The N^{2+}/H^+ abundance ratios derived using their measurements from several multiplets of the 3s–3p and 3p–3d configurations range from 4.3×10^{-4} (V 3) to 6.6×10^{-4} (V 28), while the λλ4041,4043 3d–4f transitions yield values between 7 and 8×10^{-4}. These values are somewhat higher than the values of $(3.1–3.5) \times 10^{-4}$ deduced by Liu et al. (1995).

[d] The contribution from He I $2p\,^1P^o$ – $6s\,^1S$ λ4168.97 is corrected for using the He I $2p\,^1P^o$ – $5s\,^1S$ λ4437.55 line, assuming $I(\lambda4168.97)/I(\lambda4437.55) = 0.52$ (Brocklehurst 1972).
[e] Possibly contaminated by other lines.
[f] Low S/N or blended; Excluded in the calculation of the total intensity and average abundance of the multiplet.

Table 13. O^{2+}/H^+ abundances from 3d–4f recombination lines.

λ_0 (Å)	Mult	M1-42 I_{obs}	M1-42 $\frac{O^{2+}}{H^+}$ (10^{-3})	M2-36 I_{obs}	M2-36 $\frac{O^{2+}}{H^+}$ (10^{-3})
4071.23	V48a	.101	4.29	.075	3.57
4089.29	V48a	.796	5.76	.510	4.14
4083.90	V48b	.298	7.54	.201	5.70
4087.15[a]	V48c	.293	7.30	.197	5.51
4062.94	V50a	.152	8.74	.048	3.09
4273–78[b]	V67	.935	5.32	.624	3.98
4281–84[c]	V53,67	.301	6.17	.195	4.48
4303.83[d]	V53a	.531	7.92	.293	4.90
4317.70[e,p]	V53a	.103	10.5	.036	4.11
4294.78,.92	V53b	.205	5.18	.141	4.00
4307.23	V53b	.099	6.83	.052	4.02
4288.82	V53c	.101	7.31	.033	2.68
4291–92[f]	V55,78c	.227	6.44	.150	4.77
4357.25[g,p]	V63a	.085	10.7	.057	8.08
4334.19[h,p]	V63b	.109	13.3	.047	6.44
4315.40[i]	V63c	.112	7.27	.064	4.65
4331.13	V65b	.083	7.77	.052	5.46
4332.71	V65b	.103	7.81	.072	6.12
4371.62[j]	V76b	.082[p]	6.09	.091	7.58
4353.59[k]	V76c	.093	6.41	.055	4.25
4313.44[l]	V78a	.171	6.76	.094	4.16
4285.69	V78b	.132	5.03	.104	4.44
4491.23	V86a	.123	6.49	.068	4.02
4466.42[m]	V86b	.103	7.31	.066	5.25
4489.49	V86b	.059	6.52	.038	4.71
4477.90	V88	.078	6.56	.055	5.19
4669.27[n]	V89b	.047	8.40	.027	5.44
4609.44	V92a	.404	6.81	.208	3.93
4602.13	V92b	.197	8.33	.094	4.46
4613.68[o,p]	V92b	.143	8.33	.066	4.46
4610.20	V92c	.082[p]	4.26	.093	5.42
Sum		**5.49**	**6.48**	**3.55**	**4.46**

[a] Includes a 6.6 per cent contribution from O II $3d\,^4F_{9/2}$ – $4f\,G[5]_{9/2}$ 4088.27 (V 48a).
[b] Includes 11 O II 3d–4f transitions.
[c] Includes O II $3d\,^4P_{5/2}$ – $4f\,D[2]_{5/2}$ λ4281.32 (V 53b), $3d\,^4P_{5/2}$ – $4f\,D[2]_{3/2}$ λ4281.46 (V 53b), $3d\,^2F_{5/2}$ – $4f\,F[4]_{7/2}$ λ4282.02 (V 78a), $3d\,^4D_{3/2}$ – $4f\,F[2]_{5/2}$ λ4282.96 (V 67c), $3d\,^4D_{5/2}$ – $4f\,F[2]_{5/2}$ λ4283.25 (V 67c), $3d\,^4D_{3/2}$ – $4f\,F[2]_{3/2}$ λ4283.73 (V 67c), $3d\,^4D_{5/2}$ – $4f\,F[2]_{3/2}$ λ4284.00 (V 67c), and $3d\,^4D_{7/2}$ – $4f\,F[2]_{5/2}$ λ4284.39 (V 67c).
[d] Includes a 15 per cent contribution from O II $3d\,^4D_{5/2}$ – $4f\,G[5]_{9/2}$ λ4303.61 (V 65a) and $3d\,^4P_{5/2}$ – $4f\,D[3]_{5/2}$ λ4304.08 (V 53a).
[e] Affected by O II λ4317.14 (V 2).
[f] Includes O II $3d\,^4P_{5/2}$ – $4f\,G[3]_{7/2}$ λ4291.25 (V 55), $3d\,^4P_{5/2}$ – $4f\,G[3]_{5/2}$ λ4291.86 (V 55), $3d\,^2F_{5/2}$ – $4f\,F[2]_{5/2}$ λ4292.21 (V 78c) and $3d\,^2F_{5/2}$ – $4f\,F[2]_{3/2}$ λ4292.95 (V 78c).
[g] Includes a 13 per cent contribution from O II $3d\,^4D_{3/2}$ – $4f\,D[3]_{5/2}$ λ4357.25 (V 63a).
[h] Includes the contributions from O II (V 63b) $3d\,^4D_{3/2}$ – $4f\,D[2]_{3/2}$ λ4334.33, $3d\,^4D_{3/2}$ – $4f\,D[2]_{3/2}$ λ4335.36 and $3d\,^4D_{5/2}$ – $4f\,D[2]_{3/2}$ λ4334.03. This line must have been contaminated by strong line H5 λ4340.46 and O II line λ4336.86(V2).
[i] Includes a 58 per cent contribution from O II $3d\,^4D_{3/2}$ – $4f\,D[1]_{1/2}$ λ4315.39 (V 63c), $3d\,^2F_{7/2}$ – $4f\,F[3]_{5/2}$ λ4315.39 (V 78b), $3d\,^4D_{5/2}$ – $4f\,D[1]_{3/2}$ λ4315.69 (V 63c) and $3d\,^2F_{7/2}$ – $4f\,F[3]_{7/2}$ λ4315.83 (V 78b).
[j] Includes O II λ4372.10.
[k] Includes a 3 per cent contribution from O II $3d\,^2F_{5/2}$ – $4f\,G[3]_{5/2}$ λ4354.18 (V 76c).
[l] Includes a 34 per cent contribution from O II $3d\,^2F_{7/2}$ – $4f\,F[4]_{7/2}$ λ4312.11 (V 78a).
[m] Includes a 11 per cent contribution from O II $3d\,^2P_{3/2}$ – $4f\,D[2]_{3/2}$ λ4466.59 (V 86b).
[n] Includes a 45 per cent contribution from O II $3d\,^2D_{3/2}$ – $4f\,D[2]_{3/2}$ λ4669.43 (V 89b).
[o] Includes V92b O II λ4613.14 and N II V5 λ4613.87. The intensity of O II lines is derived by using I(λ4613.68 + λ4613.14)/I(λ4602.13 = 0.453; $3d\,^2D_{3/2}$ – $4f\,F[2]_{3/2}$ λ4611.07 (V 92c).
[p] With low S/N or blended with other lines, not included in calculating the average abundance.

It has been known for some time that N II permitted lines from the low lying 3s–3p and 3p–3d triplet terms, whose upper levels are linked to the ground $2p^2\,^3P_0$ state by resonance lines, can be enhanced by fluorescence excitation. Grandi (1976) used photoionization models to study the excitation mechanisms of permitted transitions from common heavy element ions observed in the spectra of the H II region M 42 (the Orion nebula) and the PN NGC 7027 and 7662. He found that while the N II multiplet V 28 at 5942 Å is excited by both recombination and continuum fluorescence of starlight, the N II multiplets V 3 $3s\,^3P^o$–$3p\,^3D$ λ5630, V 5 $3s\,^3P^o$–$3p\,^3P$ λ4631 and V 30 $3p\,^3P$–$4s\,^3P^o$ λ3838 are dominated by fluorescence excitation of the N II $4s\,^3P^o_1$ level by the He I $1s^2\,^1S$–$1s8p\,^1P^o$ resonance line at 508.643 Å, which coincides in wavelength with the N II $2p^2\,^3P_0$–$4s\,^3P^o_1$ resonance line at 508.668 Å. Fluorescence excitation, line or continuum, however, cannot excite the singlet transitions or transitions from the 3d–4f configuration, given the large angular momenta of the upper levels of the latter transitions. Using our unpublished deep long-slit spectra of the Orion nebula obtained at the Anglo-Australian Telescope (AAT) and the ESO 1.52-m telescopes, we derive a N^{2+}/H^+ abundance ratio of 4.47×10^{-5} from the N II λλ4041, 4043 3d–4f transitions.[2] The result is consistent with the non-detection of the *singlet* transitions $3d\,^1F^o$–$4f'\left[4\tfrac{1}{2}\right]$ λ4530 (multiplet V 58) and $3s\,^1P^o$–$3p\,^1D$ λ3995 (multiplet V 12), which yields an upper limit of $N^{2+}/H^+ \lesssim 6\times10^{-5}$. In contrast, the 3s–3p multiplet V 5 yields a N^{2+}/H^+ abundance ratio five times higher than the value derived from the 3d–4f λλ4041,4043 lines. Other low-excitation triplet multiplets, such as V 5 from the 3s–3p configuration and V 20, V 28 and V 29 from the 3p–3d configuration also yield high abundances. These results are in line with Grandi's conclusion that apart from recombination, additional mechanisms are contributing to the excitation of the N II 3s–3p and 3p–3d triplet transitions observed in the spectrum of the Orion nebula.

For the scenario of He I resonance line fluorescence, as proposed by Grandi (1976), the excited N II $4s\,^3P^o_1$ level will mainly decay (apart from resonance scattering) to the $3p\,^3D_2$ level by emitting a photon at 3331.310 Å (multiplet V 22, $A_{21} = 8.3\times10^7\ s^{-1}$), or via the transitions $3p\,^3S_1$–$4s\,^3P^o_1$ λ3609.097 (multiplet V 26, $A_{21} = 2.4\times10^7\ s^{-1}$) and $3p\,^3P_1$–$4s\,^3P^o_1$ λ3847.409 (multiplet V 30, $A_{21} = 1.5\times10^7\ s^{-1}$). Thus if He I resonance line fluorescence dominates, we would expect these lines to be stronger than, for example, transitions from multiplets V 3 and V 5, which fall further down the cascade ladder. None of these lines are detected in the spectra of M 42 published by Esteban et al. (1998). A flux upper limit of $\lesssim 1\times10^{-4}$ relative to Hβ for the λ3609 and λ3847 transitions is obtained from our unpublished observations of M 42. The upper limit is lower than the observed fluxes of the strongest components of multiplets V 3 and V 5, which ranges from 3 to 5×10^{-4}. Thus our observation does not seem to

[2] Esteban et al. (1998) recently published line fluxes in the 3500–7060 Å range for two regions of the Orion nebula, using high-resolution spectra obtained with an echelle spectrograph and a CCD detector. Their spectra were however not deep enough to see the N II λλ4041,4043 lines.

Table 14. Observed intensities of O II ORLs, relative to V 48a, λ4089.

	Transition		NGC 7009			M 2-36	NGC 6153		M 1-42	Mean
			PA00 CCD	PA45 IPCS	PA45 CCD		Minor-axis	Whole Nebula		
V 1	$3s\,^4P_{5/2}$–$3p\,^4D^o_{7/2}$	λ4649	2.59	2.77	2.43	2.66	2.52	2.54	2.21	2.53 ± 0.18
V 10	$3p\,^4D^o_{5/2}$–$3d\,^4F_{7/2}$	λ4072	1.99	1.96	2.03	1.89	1.78	1.89	1.63	1.88 ± 0.14
V 48a	$3d\,^4F_{9/2}$–$4f\ G[5]^o_{11/2}$	λ4089	1.00	1.00	1.00	1.00	1.00	1.00	1.00	1.00
V 15	$3s'\,^2D$–$3p'\,^2F^o$	λλ4590,4596	0.52	0.55	0.48	0.41	0.44	0.44	0.27	0.44 ± 0.09
V 36	$3p'\,^2F^o$–$3d'\,^2G$	λλ4185,4190	0.50	0.43	0.52	0.35	0.32	0.31	0.17	0.37 ± 0.12
V 101	$3d'\,^2G$–$4f'\ H[5]^o$	λ4254	0.12	0.12	0.10	0.16	0.07	0.11		0.11 ± 0.03
	T_e(BJ) (K)			8150		5900	6080		3560	
	O^{2+}(ORL)/O^{2+}(CEL)			4.7		6.9	9.2		22	

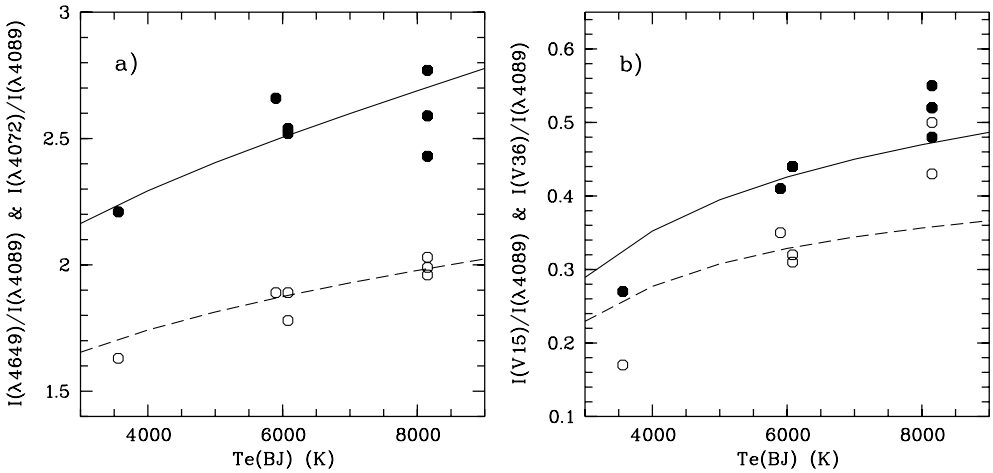

Figure 6. (a) The observed intensities of the O II transitions V 1 $3s\,^4P_{5/2}$–$3p\,^4D^o_{7/2}$ λ4649 (filled circles) and V 10 $3p\,^4D^o_{5/2}$–$3d\,^4F_{7/2}$ λ4072 (open circles), relative to the V 48a $3d\,^4F_{9/2}$–$4f\ G[5]^o_{11/2}$ λ4089 line, are plotted against the nebular Balmer jump temperature T_e(BJ). The solid and dashed lines show respectively, the predicted intensity ratios of $I(\lambda4649)/I(\lambda4089)$, multiplied by a factor of 0.63, and $I(\lambda4072)/I(\lambda4089)$, multiplied by a factor of 0.95, as a function of electron temperature. An electron density of $N_e = 3000\,cm^{-3}$ was assumed. (b) Same as (a) but for the O II $3s'\,^2D$–$3p'\,^2F^o$ multiplet V 15 (filled circles) and the $3p'\,^2F^o$–$3d'\,^2G$ multiplet V 36 (open circles). The solid and dashed lines are respectively, the predicted intensity ratios of $I(V\,15)/I(\lambda4089)$, multiplied by a factor of 1.68, and $I(V\,36)/I(\lambda4089)$, multiplied by a factor of 0.68, as a function of electron temperature. We assume that multiplets V 15 and V 36 are excited by (resonant) dielectronic recombination only, with their effective recombination coefficients given by Nussbaumer & Storey (1984).

support the He I resonance line fluorescence proposed by Grandi (1976) as the source of enhancement of low-lying N II triplet lines. Continuum fluorescence by starlight may be a more attractive mechanism, although further calculations are needed to clarify the situation. Further observation of the [N II] λ3331 transition, the main product of the He I line fluorescence mechanism, that was not covered in our spectrum of the Orion nebula, may also be useful.

It appears that the N II 3s–3p and 3p–3d transitions in M 1-42 and M 2-36 have also been enhanced by fluorescence excitation, though to a lesser extent than in the Orion nebula. However, as in the case of the Orion nebula, the He I resonance line fluorescence mechanism proposed by Grandi (1976) as the source of enhancement is questionable, as we failed to detect the N II λ3331, λ3609 and λ3847 lines from either PN. For M 2-36, the upper limits estimated for these three transitions are respectively 0.1, 0.03 and 0.03 (in units where $H\beta = 100$), compared with the observed intensity of 0.388 for the λ5680 line, the strongest component of the 3s–3p V 3 multiplet. Similarly, for M 1-42, the upper limits for the λ3331, λ3609 and λ3847 lines are 1, 0.2 and 0.06, respectively compared with the enormous value of 1.27 measured for the λ5680 line.

Given the possible enhancement of the low-lying N II triplet transitions by excitation mechanisms other than recombination, we will adopt the N^{2+}/H^+ ratios derived only from the 3d–4f transitions for both nebulae.

5.2.4 O^{2+}/H^+ abundances from ORLs

The O^{2+}/H^+ abundance ratios derived from O II ORLs are presented in Table 12 for the 3–3 transitions and in Table 13 for the 3d–4f lines. The O II ORL spectrum detected in M 1-42 is phenomenal, yielding the highest O II line intensities (relative to Hβ) ever seen in a PN. The relative intensities of individual multiplets, doublets or quartets, and multiplet transitions from the 3d–4f group closely resemble those observed from NGC 7009 (Liu et al. 1995) and 6153 (Paper I), with excellent agreement among the O^{2+}/H^+ abundances derived from the 3p–3d and 3d–4f

transitions.[3] As in the case of NGC 7009 and 6153, the two triplet 3s–3p multiplets, V 1 and V 2, particularly the second one, yield lower abundances compared to other transitions. While V 1 is insensitive to optical depth effects, assuming Case A recombination would increase the O^{2+}/H^+ abundance derived from V 2 by 40 per cent compared to the Case B value adopted in the current analysis.

The mean O^{2+}/H^+ abundance ratios and standard errors derived by averaging the values from all 3–3 multiplets (excluding the result from V 33) together with the co-added 3d–4f transitions (the values in boldface in Table 13) are (5.59 ± 0.48) and $(3.76 \pm 0.20) \times 10^{-3}$ for M 1-42 and M 2-36, respectively. These values will be adopted in our following discussion.

Recently Dinerstein et al. (2000) measured O II ORLs from a dozen PN, using CCD spectra obtained with the 2.7-m telescope of the McDonald Observatory. The spectra covered the 4020–4720 Å wavelength region at a resolving power of 1800. They found that there is a large scatter among the O^{2+}/H^+ abundance ratios derived from individual O II ORLs at the same nebular position. However, more importantly, they found that the degree of scatter varies from target to target and was largest for the doubly excited multiplet V 15, $3s'\,^2D$–$3p'\,^2F^o$ at 4590 and 4596 Å. They suggest that an unidentified mechanism is selectively enhancing the O II ORLs, in particular those from doubly excited states. They speculated, for example, that high temperature dielectronic recombination, or transient ionized regions produced by a passing shock wave or ionization front may be candidates for such a mechanism currently not included in the analysis of the O II recombination line spectrum.

As discussed in some detail in Paper I, most recent calculations of effective recombination coefficients for line emission in light elements (Storey 1994; Liu et al. 1995; Kisielius et al. 1998; Davey et al. 2000) all rely on bound–bound and bound-free radiative data calculated using the R-matrix method. In the case of O II, first calculated by Storey (1994) assuming *LS*-coupling and then by Liu et al. (1995) assuming intermediate coupling for the 3p–3d and 3d–4f configurations, the R-matrix method was used for states up to valence electron principle quantum number $n = 10$, including contributions from both radiative and dielectronic recombinations. For $n > 10$ more approximate methods are used, and in particular dielectronic recombination is not included. For dielectronic recombination excitation of levels $n > 10$ to become effective, temperatures of $(2–5) \times 10^4$ K are required. While it is possible that some nebulae may harbor pockets of hot gas, making them possible sites for high-temperature dielectronic recombination, a detailed evaluation of the significance of this process is not feasible at present because of the lack of relevant atomic data.

O II $3s'\,^2D$–$3p'\,^2F^o$ multiplet V 15 has a parentage $2p^2\,^1D$ level, thus its excitation is probably dominated by dielectronic, rather than radiative recombination. Reliable effective recombination coefficients needed to analyse these doubly excited transitions are not available. It was for this reason that all O II ORLs with parentage other than the ground level of O^{2+}, $2p^2\,^3P$, have not been included in our O^{2+}/H^+ ORL abundance analyses so far. Nevertheless, in the light of the recent work by Dinerstein et al., it is of some interest to investigate the intensities of these transitions relative to the 'normal' lines from the singly excited states, in particular from objects such as NGC 6153 and M 1-42, where the discrepancies between O^{2+}/H^+ abundances derived from ORLs and CELs are the largest.

Apart from V 15, multiplets V 36 $3p'\,^2F^o$–$3d'\,^2G$ λλ4185,4190 and V 101 $3d'\,^2G$–$4f'H[5]^o$ λ4254 have also been detected from NGC 7009 (Liu et. al. 1995), 6153 (Paper I) and from M 1-42 and M 2-36 (Table 2). Together, they form the primary transition series from spectral terms with a $2p^2\,^1D$ core. For pure *LS*-coupling, the two components of V 15, at 4590.974 ($J = 5/2$–$7/2$) and 4596.163 Å (blend of the $J = 3/2$–$5/2$ and $J = 5/2$–$5/2$ components), and the two components of V 36, at 4189.782 (blend of the $J = 7/2$–$9/2$ and $J = 7/2$–$7/2$ components) and 4185.440 Å ($J = 5/2$–$7/2$) have an intensity ratio of 4:3, which is in good agreement with that observed. All three components of V 101 blend together and have an average wavelength of 4253.996 Å.

The observed intensities of multiplet V 15, V 36 and V 101, relative to $3d\,^4F_{9/2}$–$4f\,G[5]^o_{11/2}$ λ4089, the strongest transition from the 3d–4f configuration[4] are presented in Table 14 for NGC 7009 (Liu et al. 1995), 6153 (Paper I) as well as for M 1-42 and M 2-36.

The λ4596 line has not been detected from M 1-42 and the total intensity of multiplet V 15 from this nebula was calculated from the intensity of the λ4590 line assuming that λ4590 and λ4596 have an intensity ratio of 4:3. Also given in Table 14 are the observed intensities for the $3s\,^4P_{5/2}$–$3p\,^4D^o_{7/2}$ λ4649 line, the strongest transition from the 3s–3p group, and for the $3p\,^4D^o_{5/2}$–$3d\,^4F_{7/2}$ λ4072 line, the second strongest transition from the 3p–3d configuration. The strongest transition from the 3p–3d group, λ4075.86 of V 10, was not used because it is blended with the [S II] λ4076.35 line and is consequently more difficult to measure (cf. Fig. 2 and Section 5.1.4 of Liu et al. 1995). The average intensity ratios, along with their standard *deviations*, are given in the last column of Table 14. In the last two rows of Table 14, we list for each nebula the Balmer jump temperature T_e(BJ) and the ratio of the O^{2+}/H^{2+} abundances derived from O II ORLs and from the [O III] λλ4959, 5007 forbidden lines.

Table 14 shows that, in all cases, the intensities of the O II multiplets V 15, V 36 and V 101 from the doubly excited states, as well as those of the λ4649 and λ4072 lines from the 'normal states', observed in the four nebulae are remarkably constant relative to the λ4089 transition. In the case of λ4649 and λ4072, their observed intensities relative to λ4089 stray over a range of only 10 per cent around their mean values, even though the observed discrepancies between the O^{2+}/H^+ abundances derived from ORLs and from CELs span a wide range, from approximately

[3] Except for multiplet V 33i, which yields a much higher abundance. The result is, however, based on two marginally detected lines. In NGC 6153, V 33 was also only marginally detected in the spectrum taken along the nebular minor axis, again yielding a higher abundance than those derived from other multiplets. Thus contamination by some unknown transitions seems to be the most likely cause of the discrepancy. No obvious candidates for the blending lines are known to us. Hyung & Aller (1995b) identified a weak feature at 4942.66 Å, detected in their spectrum along the minor axis of NGC 7009, as N II 4942.47 (multiplet V 7). However, the N II $3s\,^3$–$3p\,^1D$ V 7 multiplet actually has a wavelength of 3408.127 Å – clearly a misidentification.

[4] Transitions from the the 3d–4f configuration, because of their relatively high orbital angular momenta, are highly hydrogenic in nature and their effective recombination coefficients are essentially independent of optical depth and thus can be calculated with a very high accuracy. The λ4089 transition has the additional advantage that its upper level has the highest possible total angular momentum quantum number, $J = 11/2$, for an 4f state, and as a consequence, its effective recombination coefficient is independent of the coupling scheme. Together with its reasonable strength and detectability, this make λ4089 the line of choice for the purpose of abundance determinations.

a factor of 5 (NGC 7009 and M 2-36) to more than a factor of 20 (M 1-42). A slightly larger range of variations is seen in the case of the doubly excited multiplets V 15 and V 36, amounting to 80 per cent, which is probably consistent with the assumption that these doubly excited multiplets are dominated by dielectronic recombination excitation. Also consistent with this is the weakness of the $3d'\,^2G$–$4f'H[5]^o$ λ4254 multiplet, suggesting that there is an additional mechanism populating the $3p'\,^2F^o$ and $3d'\,^2G$ terms, the upper levels of multiplets V 15 and V 36.

A closer scrutiny of Table 14 shows however that the small variations seen in the intensities of these multiplets relative to λ4089 are not random but are correlated with the nebular electron temperature. In Fig. 6, the observed intensities of these multiplets relative to λ4089 are plotted against the nebular Balmer jump temperature. In Fig. 6(a) the theoretical ratios of λ4649/λ4089 and λ4072/λ4089 as a function of electron temperature are also shown, calculated using the effective recombination coefficients of Storey (1994; for the λ4649 line) and Liu et al. (1995; for the λ4072 and λ4089 lines). After multiplying the theoretical λ4649/λ4089 and λ4072/λ4089 ratios by, respectively, a *constant* factor of 0.63 and 0.95, the observed small variations of the intensities of λ4649 and λ4072 lines relative to λ4089 as a function of electron temperature follow the theoretical predictions remarkably well.

The effective (low-temperature) dielectronic recombination coefficients of multiplets V 15 and V 36 have previously been calculated by Nussbaumer & Storey (1984). Assuming that excitation by (direct) radiative recombination is negligible, which is probably a good approximation for these primed transitions, the predicted intensities of multiplets V 15 and V 36 relative to λ4089 as a function of electron temperature are plotted in Fig. 6(b) as the solid and dashed lines, respectively. For V 15, the predicted intensities are systematically lower than those observed, by approximately 40 per cent in M 1-42 and 80 per cent in NGC 7009. The inverse is true for V 36, i.e. the effective dielectronic recombination coefficients given by Nussbaumer & Storey (1984) yield intensities which are too large compared to the observed values, by approximately a factor of 2.2 in M 1-42 and a factor of 1.2 in NGC 7009.[5] In Fig. 6, in order to match the observed values for NGC 6153 and M 2-36, where both nebulae have a Balmer jump temperature of approximately 6000 K, the predicted intensities have been multiplied by *constant* values of 1.68 and 0.68 for multiplets V 15 and V 36, respectively. Considering the weakness of these primed transitions and the difficulty of calculating their effective recombination coefficients, discrepancies of less than a factor of 2 are fairly moderate, and are in any case much smaller than the discrepancies between the O^{2+}/H^+ ratios derived from O II ORLs and from [O III] CELs, which range from about a factor of 5 up to a factor of over 20 for the four PN in Table 14. We conclude that the observed intensities of these primed transitions from doubly excited states are largely consistent with those of 'normal' transitions and with the high O^{2+}/H^+ abundances yielded by the latter.

The variations as a function of electron temperature observed in the intensities of V 15 and V 36 relative to λ4089 are steeper than predicted by the calculations of Nussbaumer & Storey (1984). The *f* parameter in the exponential term of Nussbaumer & Storey's (1984) analytical fits to the effective dielectronic recombination coefficients has a value of 3498 K for V 15 and V 36, suggesting that for both multiplets the excitation is dominated by cascades from autoionizing levels which fall about 2400 cm^{-1} above the ionization limit. It is possible that recombination via some autoionizing levels of higher excitation energy may also contribute to the excitation of V 15 and V 36, leading to a steeper dependence of their emissivities on electron temperature than that predicted by Nussbaumer & Storey.

An important result from our previous analysis of the rich O II ORL spectrum observed from NGC 7009 (Liu et al. 1995) was that there is excellent agreement amongst the O^{2+}/H^+ abundances derived from a multitude of transitions, doublets or quartets. The agreement among values yielded by lines from the 3p–3d and 3d–4f configurations was particularly good. Such a good agreement however is only reached when the departure of the 3p–3d and 3d–4f transitions from pure *LS*-coupling has been taken into account, by adopting effective recombination coefficients calculated in full intermediate coupling. We also find that the O^{2+}/H^+ abundances yielded by some quartet multiplets from the lower excitation energy 3s–3p configuration, for which only *LS*-coupling effective recombination coefficients are available, are systematically *lower* (i.e. contrary to the expectations of fluorescence excitation) than those derived from the 3p–3d and 3d–4f lines, by approximately 60 per cent. The origin of this discrepancy is unclear. One possibility considered by Liu et al. (1995) is the breakdown of the *LS*-coupling scheme for higher states, even though *LS*-coupling may still be a good approximation for the 3s–3p configuration. The breakdown of *LS*-coupling amongst 3p–3p and 3d–4f states can result in decays directly to the ground configuration by bypassing the $(^3P)\,3p$ terms. These are otherwise not allowed in pure LS-coupling, and as a consequence, reduce the effective recombination coefficients of the 3p levels. As an example, while forbidden in *LS*-coupling, the $n\mathrm{d}\,^4D$ levels can decay directly to the $2p^3\,^4S^o$ ground state in intermediate coupling, thus reducing the branching ratios to levels in the 3p configuration. The constancy of the intensity ratio of the 3s–3p transition λ4649 to the 3d–4f transition λ4089, after the small variations with temperature predicted by recombination theory have been taken out, and the excellent agreement between the observed and predicted λ4072/λ4089 ratios,[6] seem to support this interpretation.

In summary, the small variations observed in the intensity ratios of 'normal' O II ORLs from singly excited states are well accounted for by current recombination theory. The observed intensities of multiplets V 15 and V 36 from the doubly excited states, relative to the λ4089 line from the singly excited state, are also in good agreement with those predicted using the effective dielectronic recombination coefficients calculated by Nussbaumer & Storey (1984), although the emissivities of these primed transitions as a function of electron temperature are found to be slightly steeper than those predicted by Nussbaumer & Storey. Nevertheless, there is no evidence in our data to support the claims

[5] In the calculations of Nussbaumer & Storey (1984), approximately one third of the population of $3p'\,^2F^o$, the upper level of V 15, is diverted to the UV transition, $2p^4\,^2D$–$3p'\,^2F^o$, resulting in an effective recombination coefficient of V 15 which is smaller than that of V 36.

[6] Liu et al. (1995) noted that there is some evidence that the observed λ4072/λ4075 intensity ratio is higher than that predicted by recombination theory, and suggested that the λ4072 line may be contaminated by some unknown line. That the observed λ4072/λ4075 ratio is larger than predicted seems to be supported by measurements from NGC 6153, M 1-42 and M 2-36. However, given the excellent agreement of the observed λ4072/λ4089 ratios with the theoretical predictions in *all* four nebulae, it now seems highly unlikely that the abnormal λ4072/λ4075 ratio is caused by contamination of the λ4072 line by another, unidentified, line.

Table 15. Ne^{2+}/H^+ abundances from recombination lines.

λ_0 (Å)	Mult	M1-42 I_{obs}	M1-42 $\frac{Ne^{2+}}{H^+}$ (10^{-3})	M2-36 I_{obs}	M2-36 $\frac{Ne^{2+}}{H^+}$ (10^{-3})
3694.21	V1	.452	1.39	.460	1.41
3709.62	V1			.181	1.40
3766.26	V1			.154	1.12
3777.14	V1	.116	.915	.087	.685
V 1 $3s\,^4P - 3p\,^4P$		**1.16**	**1.25**	**1.13**	**1.22**
3327.15	V2			.061	.338
3334.84	V2	1.15	1.67	.590	.876
3355.02[a]	V2	.824	1.84	.395	.769
3360.60	V2			.080	.577
3297.37	V2			.069	.441
V 2 $3s\,^4P - 3p\,^4D$		**2.96**	**1.73**	**1.20**	**.714**
3481.93	V6			.078	.846
V 6 $3s\,^2P - 3p\,^2S$			**.117**	**.846**	
3323.74	V7			.178	.623
3378.22	V7			.048	.427
V 7 $3s\,^2P - 3p\,^2P$			**.291**	**.567**	
3568.50	V9	.342	19.0	.090	3.11
3574.18	V9			.057	2.66
V 9 $3s'\,^2D - 3p'\,^2F$			**.147**	**2.92**[r]	
3320.00[b,r]	V12			.097	9.58
3329.16	V12			.131	2.16
3386.22	V12			.023	1.89
V 12 $3p\,^4D - 3d\,^4D$			**.371**	**2.11**	
3208.96[c,r]	V13			.136	2.78
3213.73,14.33	V13			.132	.426
3218.19	V13	1.15	2.62	.545	1.28
3244.09	V13			.346	1.20
V 13 $3p\,^4D - 3d\,^4F$		**3.28**	**2.62**	**1.19**	**1.01**
3117.98[d]	V16			.205	5.62
V 16 $3p\,^4D - 3d\,^4P$			**.513**	**5.62**[r]	
3367.224[e]	V20			.140	.427
3388.42	V20			.088	.386
V 20 $3p\,^2D - 3d\,^2F$			**.235**	**.410**	
3416.91[f,r]	V21	.308	4.67	.161	2.52
3453.07	V21			.060	1.48
3477.65[g,r]	V21			.057	12.7
V 21 $3p\,^2D - 3d\,^2D$			**.167**	**1.48**	
	3d – 4f transitions				
4219.74[h]	V52a	.178	3.32	.125	2.33
4233.85	V52a	.032	2.39	.032	2.39
4231.64[i]	V52b			.046	3.62
4250.65	V52b			.029	3.42
4391.99[j]	V55e	.179	1.85	.148	1.53
4409.30	V55e	.156	2.43	.127	1.98
4397.99	V57b	.033	0.99	.051	1.53
4428.64[k]	V60c	.088	2.09	.088	2.09
4430.94[l]	V61a	.128	4.69	.071	2.60
4457.05[m,r]	V61a	.085	8.93	.040	4.20
4413.22[n]	V65	.107	4.63	.068	2.94
Sum		**.901**	**2.55**	**.785**	**2.09**

[a] Corrected for the contribution from the He I $2s^1S$-$7p^1P°$ λ3354.55 line assuming I(λ3355/I(λ3613) = 0.35. The corrections are 20 and 32 per cent for M 1-42 and M 2-36 respectively.
[b] The observed wavelength of this transition is 3320.86 Å, possibly contaminated by some other unknown lines.
[c] Blending with Ne II $3p\,^4D$–$3d\,^4P$ λ3209.36.
[d] Possibly contaminated by other additional Ne II transitions at the similar wavelength.
[e] Neglecting Ne II $3p\,^4D_{5/2}$–$3d\,^4D_{7/2}$ λ3366.98.
[f] Blending with the O III Bowen fluorescence line λ3415.29 and Ne II $2s^2p^4(^3P)3p\,^2D^o_{5/2}$–$2s^2p^4(^3p)3d\,^4F_{7/2}$ λ3417.69.
[g] Probably contaminated by some unknown lines.
[h] Neglecting Ne II $3d\,^4D_{7/2}$–$4f\,2[4]_{7/2}$λ4219.37 (V 52a), which may contribute a few per cent of the observed intensity.
[i] Neglecting Ne II $3d\,^4D_{5/2}$–$4f\,2[3]_{5/2}$λ4231.53 (V 52b).
[j] Neglecting Ne II $3d\,^4F_{9/2}$–$4f\,2[5]_{9/2}$λ4392.00 (V 55e).
[k] Including the contributions from Ne II $3d\,^2D_{5/2}$–$4f\,2[3]_{7/2}$ λ4428.52 (V 61b); but neglecting $3d\,^2F_{5/2}$–$4f\,1[3]_{5/2}$ λ4428.52 (V 60c).
[l] Including Ne II $3d\,^4F_{3/2}$–$4f\,1[2]_{5/2}$ λ4430.90 (V 57a).
[m] Neglecting Ne II $3d\,^2D_{3/2}$–$4f\,2[2]_{3/2}$λ4457.24 (V 61d).
[n] Neglecting Ne II $3d\,^4P_{5/2}$–$4f\,0[3]_{5/2}$λ4413.11 (V 65) and $3d\,^4F_{3/2}$–$4f\,1[3]_{5/2}$ λ4413.11 (V 57c).
[r] Not included in calculating the total intensity of the multiplet and the average abundance.

by Dinerstein et al. (2000) that there is a large scatter among the O^{2+}/H^+ abundances derived from individual O II multiplets and that the magnitude of the scatter varies from target to target and tends to increase with the increase of the discrepancy between the O^{2+}/H^+ abundances derived from ORLs and CELs.

5.2.5 Ne^{2+}/H^+ *abundances from ORLs*

Several Ne II multiplets, including a number of transitions from the 3d–4f configuration have been detected. The Ne^{2+}/H^+ values derived from them are presented in Table 15. Ne II has a doublet ground state, $2p^5\,^2P^o$. Of the several doublet multiplets detected, the emissivities of multiplets V 6, V 7 and V 21 are sensitive to the optical depths of the Ne II resonance lines, and Case B recombination has been assumed in calculating Ne^{2+}/H^+ abundances from their observed intensities. The fact that the resultant values agree closely with those derived from quartet transitions, which are essentially case insensitive, indicates that Case B recombination is a good approximation for the doublet states.

The Ne^{2+}/H^+ abundance for M 1-42 derived from multiplet V 21 was based on a single (weak) transition and is significantly higher than values deduced from other multiplets. After excluding V 21, averaging the abundances given by other 3–3 multiplets as well as by the co-added 3d–4f transitions yields a mean Ne^{2+}/H^+ abundance of 2.04×10^{-3}, which will be adopted in our further analysis.

For M 2-36, the Ne^{2+}/H^+ abundance derived from multiplet V 16 was based on a single transition close to the atmospheric cut-off. It also yields the highest value, possibly caused by contamination by other weak Ne II lines at a similar wavelength. This multiplet was excluded when calculating the average Ne^{2+}/H^+ abundance ratio. The transitions from multiplet V 9, $3s'\,^2D$–$3p'\,^2F^o$ have an excited parentage, $2s^22p^4\,^1D$. Since they involve two excited electrons, it is possible that their excitation is dominated by dielectronic recombination and the effective recombination coefficients adopted in the current analysis may have been underestimated. We have therefore ignored abundances given by this multiplet. Excluding V 16 and V 9, averaging the results presented in Table 15 yields a mean Ne^{2+}/H^+ abundance of 1.16×10^{-3} for M 2-36.

Note that as in the case of NGC 6153 (Paper I) and 7009 (Luo et al. 2001), the 3d–4f transitions yield average Ne^{2+}/H^+ abundances which are approximately a factor of 1.4 and 2.0 higher than those derived from the 3–3 transitions, in the case of M 1-42

and M 2-36, respectively, a discrepancy possibly caused by uncertainties in the effective recombination coefficients of the 3d–4f transitions (Paper I).

5.2.6 C^{3+}/H^+ and N^{3+}/H^+ abundances from ORLs

The C^{3+}/H^+ and N^{3+}/H^+ abundance ratios derived from ORLs are presented in Table 16. For C^{3+}/H^+, the values derived from multiplets V 1 and V 18 are averaged, giving a mean abundance of 7.0×10^{-5} and 1.09×10^{-4} for M 1-42 and M 2-36, respectively.

Table 16. C^{3+}/H^+ and N^{3+}/H^+ abundances from optical recombination lines.

		M1-42		M2-36	
Mult	λ_0 (Å)	I_{obs}	$\frac{C^{3+}}{H^+}$ (10^{-3})	I_{obs}	$\frac{C^{3+}}{H^+}$ (10^{-3})
V 1 $3s\,^3S-3p\,^3P$	4650	**.266**	**.078**	**.381**	**.116**
V 18 $4f\,^1F-5g\,^1G$	4186	**.047**	**.062**	**.070**	**.102**
Mult	λ_0 (Å)	I_{obs}	$\frac{N^{3+}}{H^+}$ (10^{-3})	I_{obs}	$\frac{N^{3+}}{H^+}$ (10^{-3})
V 18 $4f\,^2F-5g\,^2G$	4379[a]	**1.09**	**.371**	**.351**	**.133**

[a] Corrected for a contribution of 9 and 20 per cent from Ne II λ4379.55(V 60b) for M1-42 and M2-36 respectively, assuming Ne II I(λ4379.55)/I(λ4391.99) = 0.61.

5.2.7 The efficiency of the Bowen fluorescence mechanism

In Paper I, we noted that compared to a typical PN, both NGC 7009 and 6153 have a very high efficiency for the Bowen fluorescence mechanism. Similar results are found here for M 1-42 and M 2-36, for which we derive Bowen fluorescence efficiencies of 0.55 and 0.64, respectively.

5.3 Total elemental abundances

Total elemental abundances derived from ORLs and from CELs are presented in Table 17. They were calculated from the ionic abundances using the same procedures and ionization correction factors (ICFs) as described in Paper I. For ions whose abundances have been deduced from both optical CELs and IR fine-structure lines, results from the two determinations were averaged with equal weight.

Abundances for M 1-42 and M 2-36 have been presented by Ratag et al. (1997) who determined the chemical composition for a large sample of Galactic bulge PN, using the standard method based on collisional line analyses. Their results are listed in Table 17 for comparison. For M 1-42, their results agree reasonably well with ours except for Cl, for which they derived an abundance which is more than a factor of 2 higher. The agreement was less satisfactory for M 2-36. Apart from He, O and Ar, there are

Table 17. Elemental abundances by number, derived from CELs and ORLs, in units such that $\log N(H) = 12.0$.

	M1-42		M2-36		M 1-42	M 2-36	Average PN abundances[a]		Solar[b]
	ORLs	CELs	ORLs	CELs	Ratag et al. (1997)		Type I	non-Type I	
He	11.17		11.13		11.22	11.09	11.11	11.05	10.99
C	9.35	7.80	9.41	8.73			8.48	8.81	8.55
N	9.59	8.68	9.17	8.42	8.75	8.62	8.72	8.14	7.97
O	9.79	8.63	9.64	8.85	8.57	8.89	8.65	8.69	8.87
Ne	9.40	8.12	9.16	8.57	8.03	8.27	8.09	8.10	8.09
S		7.08		7.47	7.16	7.17	6.91	6.91	7.21
Cl		5.26		5.42	5.80	5.98			5.50
Ar		6.56		6.66	6.58	6.61	6.42	6.38	6.56

[a]Kingsburgh & Barlow (1994).
[b]Anders & Grevesse (1989) and Grevesse & Noels (1993).

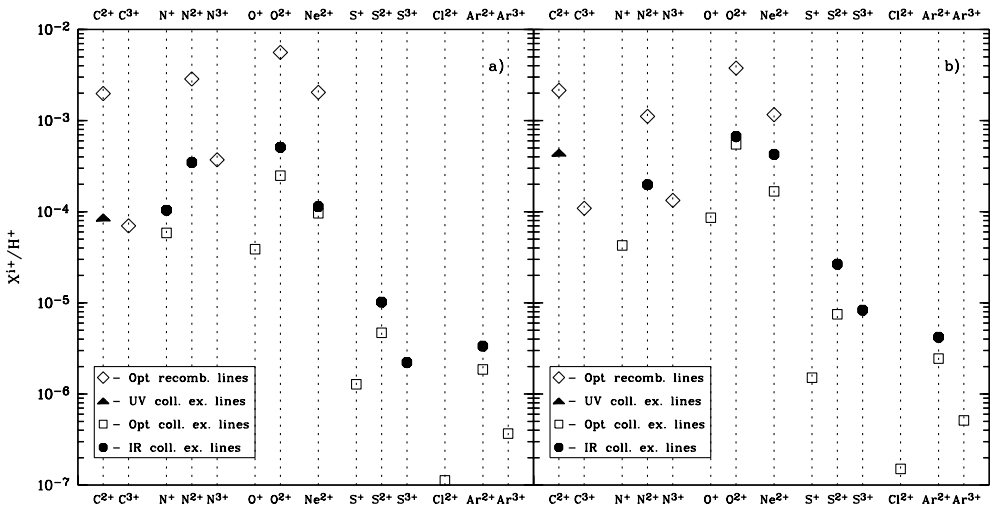

Figure 7. Comparison of ionic abundances derived from ORLs, and from UV, optical and IR CELs for (a) M 1-42 and (b) M 2-36.

Table 18. Ionic abundances derived from ORLs and CELs and their ratios. The letters U, O and R behind the CEL abundances denote, respectively, values derived from UV, optical and IR fine-structure CELs.

	M1-42			M2-36		
	ORL	CEL	*R*	ORLs	CEL	*R*
$10^5\times C^{2+}/H^+$	198	8.67U	23	214	44.6U	4.8
$10^5\times N^{2+}/H^+$	286	34.8R	8.2	111	19.8R	5.6
$10^5\times O^{2+}/H^+$	559	24.9O	22	376	54.8O	6.9
		51.0R	11		67.0R	5.6
$10^5\times Ne^{2+}/H^+$	167	9.62O	17	128	16.7O	7.7
		11.4R	15		42.7R	3.0

significant differences between the two studies – for Ne and S, our derived CEL abundances are a factor of 2 higher than theirs while for N and Cl, our values are respectively a factor of 1.6 and 3.6 lower.

Both M 1-42 and M 2-36 are enhanced in He and N, and can be classified as Type I PN according to the original criteria of Peimbert & Torres-Peimbert (1983), although according to Kingsburgh & Barlow's (1994) new criterion for Type I PN, which is based on the N/O abundance ratio only and requires that the observed N/O abundance ratio to be greater than the average (N + C)/O abundance ratio (= 0.8) for Galactic H II regions, only M 1-42, for which we find N/O = 0.63 and 1.12 from the ORL and CEL analyses, respectively, may just qualify as a Type I PN. While the C/O, S/O and Ar/O abundance ratios are close to the solar values, there is some evidence that Ne is enhanced in both nebulae. Compared to the solar value of −0.79, the measured Ne/O ratios for M 1-42 and M 2-36 vary from −0.39 to −0.48 dex as determined from ORLs and from −0.51 to −0.28 as yielded by CELs.

The elemental abundances of M 1-42 derived from CELs follow the average abundances of Galactic Type I PN closely (Kingsburgh & Barlow 1994), except for C which is more depleted in M 1-42, by a factor of 5, than in an average Galactic Type I PN. In contrast, the CEL abundances of all elements measured for M 2-36, except for C, are higher than the average values for non-Type I PN. The enhancement is about 50 per cent for O, a factor of 2 for N and Ar, and amounts to a factor of 3 for Ne and S.

6 DISCUSSION

6.1 Comparison of ionic abundances derived from CELs and ORLs

The ionic abundances derived from ORLs, and from UV, optical and IR CELs, are compared in Fig. 7. For the convenience of an easy reference, the abundances plotted in Fig. 7 are reproduced in Table 18 for ionic species for which abundances have been derived from both ORLs and CELs. The O^{3+}/H^+ ratio deduced for M 1-42 from the [O IV] 25.9-μm fine-structure line has been left out, as there is no corresponding CEL abundance for comparison and the line has not been detected in M 2-36. As was the case in our previous analyses of NGC 7009 and 6153, one of the most striking features revealed by Fig. 7 is that for all the heavy element ionic species for which abundances have been derived from both ORLs and CELs, the ORL abundances are systematically higher than the CEL values. The discrepancy between the ionic abundances derived from these two types of emission line is largest for M 1-42, by more than an order of magnitude. Secondly, the ratios of ORL to CEL abundances are found to be roughly comparable for all ionic species studied, about a factor of 15 in the case of M 1-42 and a factor of 5 in M 2-36. There are however some variations in the magnitude of the discrepancies for different ions in M 1-42, ranging from a factor of 8 for N^{2+}/H^+ to as much as a factor of 23 for C^{2+}/H^+.

For NGC 6153, we find that IR fine-structure lines yield ionic abundances very similar to those from the optical CELs. In M 1-42 and M 2-36, there is however evidence that IR fine-structure CELs give systematically higher abundances than optical CELs. The difference is significant, reaching for example, a factor of 2 in the case of O^{2+}/H^+ for M 1-42, that cannot be easily explained by observational uncertainties. If we adopt the O^{2+}/H^+ ratio derived from the optical [O III] λλ4959, 5007 lines as the CEL O^{2+}/H^+ abundance, then the discrepancy between the ORL and CEL abundance ratios increases from a factor of 15 to 22, i.e. becoming comparable to the discrepancy found for C^{2+}/H^+ between its two values derived from ORLs and from UV CELs. Note that for the N^{2+}/H^+ and O^{2+}/H^+ (as well as N^+/H^+) abundance ratios derived from far-IR fine-structure lines, we have adopted the values calculated using the lower electron density yielded by the observed [O III] 88-μm/52-μm ratio, rather than using the higher density yielded by the various optical density diagnostics, although the latter was used for other IR fine-structure lines of high critical densities. Because of the relatively low critical densities of the [N III] 57-μm and [O III] 52- and 88-μm lines, adopting the higher density derived from optical diagnostics will *increase* significantly the N^{2+}/H^+ and O^{2+}/H^+ abundance ratios derived from them, by about a factor of 1.3 and 2.3 for M 1-42 for the two ionic species respectively, and by a factor of 1.4 and 2.8 in the case of M 2-36, thus leading to even higher IR fine-structure line abundances as compared to those yielded by optical CELs, even though the increased IR fine-structure CEL abundances remain significantly lower than the corresponding values deduced from ORLs. On the other hand, the Ne^{2+}/H^+ abundance ratio of M 1-42 derived from the 15.5-μm line agrees very well with that deduced from the λ3868 line. Because of the very high critical density of the 15.5-μm line, the Ne^{2+}/H^+ abundance ratio deduced from it is hardly affected whichever density is used.

6.2 Balmer jump temperatures and the role of temperature fluctuations

The more than an order of magnitude discrepancy between the ionic abundances derived from ORLs and from CELs that is observed for M 1-42 is the largest amongst all the PN analysed by us so far (Liu et al. 1999). Interestingly, M 1-42 also has the lowest Balmer jump temperature, 3560 K, that has been measured for a PN, about 5660 K lower than the temperature yielded by its [O III] forbidden line ratio. In Fig. 8, the ratios of the O^{2+}/H^+ ionic abundances derived from O II ORLs and from the [O III] *optical* forbidden lines are plotted against T_e([O III]) − T_e(BJ) for a sample of 10 PN, plus the Orion nebula H II region (M 42). For NGC 7009 and 6153, the ionic abundances derived from ORLs and CELs, and the Balmer jump and [O III] temperatures, are taken from Liu et al. (1995) and Paper I, respectively. For M 42 and the other six PN, other than M 1-42 and M 2-36, the data are from Liu et al. (1999), derived from own unpublished observations.

Fig. 8 shows that there is almost a perfect linear correlation

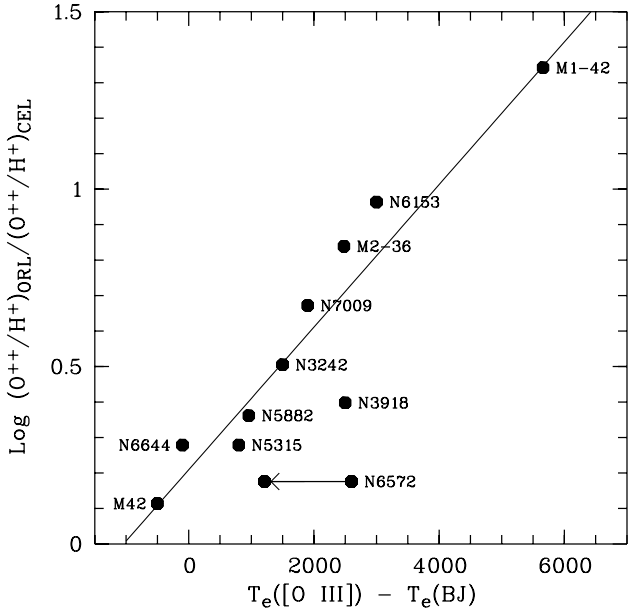

Figure 8. The ratio of O^{2+}/H^+ ionic abundances derived from ORLs and from CELs plotted against the difference between the nebular electron temperatures derived from the [O III] nebular to auroral forbidden line ratio, T_e([O III]) and from the nebular Balmer continuum discontinuity, T_e(BJ). The solid line is a linear fit to $\Delta(O^{2+}/H^+) \equiv \log(O^{2+}/H^+)_{ORL} - \log(O^{2+}/H^+)_{CEL}$ as a function of $\Delta T \equiv T_e([O\,III]) - T_e(BJ)$.

between

$$\Delta\left(\frac{O^{2+}}{H^+}\right) \equiv \log\left(\frac{O^{2+}}{H^+}\right)_{ORL} - \log\left(\frac{O^{2+}}{H^+}\right)_{CEL}$$

and

$$\Delta T \equiv T_e([O\,III]) - T_e(BJ).$$

Of the 10 PN plotted in Fig. 8, NGC 6572 has the smallest discrepancy between ORL and CEL O^{2+}/H^+ abundance ratios, $\Delta(O^{2+}/H^+) = 0.18$ (dex), yet it has fairly large temperature discrepancy, $\Delta T = 2600$ K. The Balmer jump temperature of 7800 K given by Liu et al. (1999) was derived from the ratio of the Balmer discontinuity to Hβ measured from a medium resolution spectrum obtained at the ESO 1.52-m telescope in 1992 May. Spectra in the near UV region of much better S/N and spectral resolution have been obtained by us since then. From the ratio of the Balmer jump to H 11 at 3770 Å measured from these new data, we obtain a Balmer jump temperature of 9090 K, only 1210 K lower than its [O III] forbidden line temperature. For comparison, Peimbert's (1971) original determination of the Balmer jump temperature in NGC 6572 yields 8700^{+1050}_{-900} K. It is possible that the fairly low Balmer jump temperature of NGC 6572 derived from our 1992 May data was caused by observational uncertainties. On the other hand, it is worth noting that the young, high-density nebula NGC 6572 has been known to have a peculiar and variable spectrum (Feibelman, Aller & Hyung 1992; Hyung, Aller & Feibelman 1994).

Excluding the H II region M 42 and NGC 6572, a linear fit to the nine PN plotted in Fig. 8 yields,

$$\Delta(O^{2+}/H^+) = (0.209 \pm 0.085) + (20.1 \pm 3.25) \times 10^{-5} \Delta T,$$

with a linear correlation coefficient of 0.92.

Fig. 8 provides the strongest evidence so far that the two independent observational phenomena are clearly correlated, i.e. that the Balmer jump temperature T_e(BJ) tends to be systematically lower than the [O III] forbidden line temperature T_e([O III]) (Peimbert 1971; Liu & Danziger 1993), and that the ionic abundances of heavy elements derived from ORLs are systematically higher than those derived from CELs. In other words, temperature fluctuations, as first proposed by Peimbert (1967) and used by Peimbert (1971) to interpret systematically lower Balmer jump temperature compared to [O III] forbidden line temperature, may play an important role in causing the systematically lower nebular heavy elemental abundances that are derived from CELs compared to those derived from ORLs. In terms of Peimbert's temperature fluctuation parameter t^2, since (Peimbert 1971)

$$t^2 \propto \Delta T \equiv T_e([O\,III]) - T_e(BJ),$$

the above result suggests that the magnitude of the abundance discrepancy, $\Delta(O^{2+}/H^+)$, is strongly correlated with the amplitude of the temperature fluctuations, t^2.

While the concept of temperature fluctuations provides a natural explanation for disparities in both the temperature and abundance determinations, it has several difficulties (Paper I). Apart from the fact that the underlying physical mechanisms and energy sources causing such large amplitude of temperature fluctuations are currently unknown, temperature fluctuations cannot explain the low ionic abundances yielded by IR fine-structure lines. Although collisionally excited, unlike CELs in the optical and UV wavelength regions, IR fine-structure lines have much smaller excitation energies, $E_{ex} \lesssim 1000$ K. As a result, their emissivities have only a weak, power-law dependence on T_e, $\epsilon \propto T_e^{-1/2} \exp(-E_{ex}/kT_e) \sim T^{-1/2}$ since $E_{ex} \ll kT_e$, i.e. rather similar to ORLs (for which $\epsilon \propto T_e^{-\alpha}$, where $\alpha \sim 1$), unless they arise mainly from regions with temperatures of only a few hundred K. In the case of NGC 6153, the IR fine-structure lines yield ionic abundances nearly identical to those deduced from UV and optical CELs, which are a factor of 10 lower than the corresponding ORL abundances (Paper I). For M 1-42 and M 2-36, although there is some evidence that the ionic abundances derived from the IR fine-structure lines are slightly higher than values yielded by the optical CELs, they are still far smaller than the values derived from ORLs. Simply adopting the Balmer jump temperature, rather than the [O III] forbidden line temperature, does not solve this problem. Even in the extreme case of M 1-42, T_e(BJ) = 3560 K, still significantly higher than the excitation energies of the IR fine-structure lines. Furthermore, adopting the low Balmer jump temperatures would lead to very high ionic abundances from CELs with high excitation energies, such as C III] λ1908, much higher even than the high abundance given by ORLs. This is the case even after the contribution by recombination to the intensity of the C III] λ1908 line has been taken into account (Paper I).

Density inhomogeneities containing ionized condensations with $N_e \gtrsim 10^6$ cm^{-3} can lead to apparently higher [O III] forbidden line temperature, thus mimiking the effects of temperature fluctuations (Viegas & Clegg 1994). For NGC 6153, and for M 1-42 and M 2-36 analysed here, such a possibility is essentially ruled out by the fairly low densities yielded by the high-order hydrogen Balmer decrement, unless the condensations are also H-deficient. In their empirical analysis of NGC 6153, Liu et al. (2000) find that a two-component nebular model, with H-deficient inclusions embedded in diffuse material of 'normal' metallicity, can account for many of the observed patterns. Interestingly, one of the major difficulties of such models, in particular their model IH3, where the H-deficient

condensations have very high densities ($\sim 2 \times 10^6\,\mathrm{cm}^{-3}$) but contribute only a tiny fraction of the total nebular mass (in order to satisfy the low electron density deduced from the high-order Balmer decrement), is to explain the large Balmer jump (implying a low Balmer jump temperature) that is observed in its spectrum, since in such a model, essentially all the hydrogen emission arises from the low-density, normal-temperature H-rich diffuse material. Given the very low Balmer jump temperature and yet at the same time a very low Balmer decrement density inferred for M 1-42 (cf. Table 6 and Fig. 5), we expect that such models would have difficulty in explaining the greater than a factor of 10 discrepancy between its ORL and CEL abundances.

REFERENCES

Acker A., Marcout J., Ochsenbein F., Stenholm B., Tylenda R., 1992, Strasburg-ESO catalogue of Galactic PN. European Southern Observatory, Garching bei München

Anders E., Grevesse N., 1989, Geochim. Cosmochim. Acta, 53, 197

Brocklehurst M., 1972, MNRAS, 157, 211

Brown R. L., Mathews W. G., 1970, ApJ, 160, 939

Cahn J. H., Kaler J. B., Stanghellini L., 1992, A&AS, 94, 399

Cardelli J. A., Clayton G. C., Mathis J. S., 1989, ApJ, 345, 245

Condon J. J., Kaplan D. L., 1998, ApJS, 117, 361

Crenshaw D. M., Bruegman O. W., Norman D. J., 1990, PASP, 102, 463

Davey A. R., Storey P. J., Kisielius R., 2000, A&AS, 142, 85

Dinerstein H., Lafon C. E., Garnett D. R., 2000, in Kastner J. H., Soker N., Rappaport S., eds, ASP Conf. Ser. Vol. 199, Asymmetrical Planetary Nebulae II: Origins to Microstructures. Astron. Soc. Pac., San Francisco, p. 301

Esteban C., Peimbert M., Torres-Peimbert S., Escalante V., 1998, MNRAS, 295, 401

Feibelman W. A., Aller L. H., Hyung S., 1992, PASP, 104, 339

Ferland G. J., Williams R. E., Lambert D. L., Shields G. A., Slovak M., Gondhalekar P. M., Truran J. W., 1984, ApJ, 281, 194

Grandi S. A., 1976, ApJ, 206, 658

Grevesse N., Noels A., 1993, in Prantzos N., Vangioni-Flam E., Cassé M., eds, Origin and Evolution of the Elements. Cambridge Univ. Press, Cambridge, p. 15

Howarth I. D., 1983, MNRAS, 203, 301

Hyung S., Aller L. H., 1995a, MNRAS, 273, 958

Hyung S., Aller L. H., 1995b, MNRAS, 273, 973

Hyung S., Aller L. H., Feibelman W. A., 1994, MNRAS, 269, 975

Kingsburgh R. L., Barlow M. J., 1994, MNRAS, 271, 257

Kinman T. D., Feast M. W., Lasker B. M., 1988, AJ, 95, 804

Kisielius R., Storey P. J., Davey A. R., Neale L. T., 1998, A&AS, 133, 257

Larson K. A., Whittet D. C. B., Hough J. H., 1996, ApJ, 472, 755

Liu X.-W., 1997, in Kessler M. F., ed., The First *ISO* Workshop on Analytical Spectroscopy. ESA Publication Division, ESTEC, Noordwijkerhout, p. 87

Liu X.-W., Danziger I. J., 1993, MNRAS, 263, 256

Liu X.-W., Storey P. J., Barlow M. J., Clegg R. E. S., 1995, MNRAS, 272, 369

Liu X.-W., Barlow M. J., Danziger I. J., Storey P. J., 1999, in Walsh J. R., Rosa M. R., eds, Proc. ESO Workshop on Chemical Evolution from Zero to High Redshift. Spring-Verlag, Berlin, p. 39

Liu X.-W., Storey P. J., Barlow M. J., Danziger I. J., Cohen M., Bryce M., 2000, MNRAS, 312, 585

Liu X.-W. et al., 2001, MNRAS, 323, 343

Luo S.-G., Liu X.-W., Barlow M. J., 2001, MNRAS, in press

Minkowski R., 1946, PASP, 58, 305

Minkowski R., 1947, PASP, 59, 257

Moreno H., Gutierrez-Moreno A., Torres C., Lasker B. M., 1988, PASP, 100, 604

Nussbaumer H., Storey P. J., 1984, A&AS, 56, 293

Peimbert M., 1967, ApJ, 150, 825

Peimbert M., 1971, Bol. Obs. Tonantzintla y Tacubaya, 6, 29

Peimbert M., Torres-Peimbert S., 1983, in Flower D. R., ed., Planetary Nebulae. Kluwer, Dordrecht, p. 233

Ratag M. A., Pottasch S. R., Dennefeld M., Menzies J., 1997, A&AS, 126, 297

Schneider S. E., Terzian Y., Purgathofer A., Perinotto M., 1983, ApJS, 52, 399

Smits D. P., 1996, MNRAS, 278, 683

Storey P. J., 1994, MNRAS, 282, 999

Storey P. J., Hummer D. G., 1995, MNRAS, 272, 41

Viegas S., Clegg R. E. S., 1994, MNRAS, 271, 993

Walton N. A., Barlow M. J., Clegg R. E. S., 1993, in DeJonghe H., Habing H. J., eds, Galactic bulges. Kluwer, Dordrecht, p. 337

Welty D. E., Fowler J. R., 1992, ApJ, 393, 193

Williams R. E., Woolf N. J., Hege E. K., Moore R. L., Kopriva D. A., 1978, ApJ, 224, 171

Zijlstra A. A., Pottasch S. R., Bignell C., 1989, A&AS, 79, 329

This paper has been typeset from a TEX/LATEX file prepared by the author.